NTNU – Trondheim
Norwegian University of
Science and Technology

Ultrasonic Evaluation of Well Integrity

Kristian Hoel

Petroleum Geoscience and Engineering
Submission date: June 2014
Supervisor: Rune Martin Holt, IPT
Co-supervisor: Tonni Franke Johansen, SINTEF

Norwegian University of Science and Technology
Department of Petroleum Engineering and Applied Geophysics

Abstract

This thesis presents the acoustic theory behind current ultrasonic cement evaluation tools. The UltraSonic Imager tool's pulse echo technique and the new Isolation Scanner tool's pitch-catch leaky lamb wave measuring technique is explained. A laboratory experiment is conducted on a steel casing set-up (BeCaLoS) designed by SINTEF Petroleum Research to test, and highlight weaknesses of these measuring techniques. Both evaluation methods are successfully performed under four different conditions; with air, water, mud and cement behind the steel casing. Pulse-echo wave resonance attenuation measurements prove to be successful in evaluating the physical state of the material behind the casing. Interference from the third interface echo in the resonance waveform gives good annulus thickness information. Calculated cement impedance values indicate the presence of a microannuls.

The pitch-catch plate wave attenuation measurements prove the evaluation method's weakness to thick casings. Lamb wave mode analysis is done and shows a possible mix of higher-order lamb modes present in the plate wave. Annulus material with high acoustic attenuation gave values that were difficult to interpret. The cement measurements showed low attenuation values caused by cement impedance above critical values; illustrating the importance of using both pulse-echo and pitch-catch to determine well integrity conditions. Third interface echoes were recorded successfully and gave a pretty accurate annulus thickness value. A question was raised to whether the amplitude of the initial flexural wave can be used to give information on annulus condition.

The need for cement evaluation will greatly increase in the near future, and the limitations of current tools are a cause for concern and further research in the field of cement evaluation is encouraged.

Sammendrag

Denne avhandlingen framlegger akustikk-teorien bak nåværende ultralyd sementevalueringsverktøy. UltraSonic Imager verktøyets puls-ekko teknikk og det nye Isolation Scanner verktøyets «pitch-catch» dispersiv-Lamb-bølge måleteknikk blir forklart. Et laboratorieforsøk er gjennomført på et stålplate oppsett (BeCaLoS) designet av SINTEF Petroleumsforskning for å teste og fremheve svakheter ved disse målemetodene. Begge evalueringsmetoder er utført vellykket under fire ulike forhold; med luft, vann, boreslam og sement bak stålplaten. Puls-ekko resonansbølgedempning viser seg å være egnet til å evaluere den fysiske tilstanden til materialet bak stålplaten. Forstyrrelser fra tredjegrensesnittekkoet i resonansbølgeformen gir gode målinger av borehulltykkelsen. Beregnede verdier av sementimpedans indikerer et mikroannuli mellom stålplaten og sementen.

Den målte «Pitch-Catch»-platebølgedempningen tydeliggjør metodens svakhet med hensyn til platetykkelse. En Lamb-bølgemodus analyse er gjort og viser en mulig miksing av høyereordens Lamb-modi i den observerte platebølgen. Materialer med høy akustisk dempning bak stålplaten ga verdier som var vanskelige å tolke. Sementmålinger viste lave bølgedempningsverdier forårsaket av at sementimpedansen var over en kritisk verdi. Dette framhever betydningen av å bruke både puls-ekko og «pitch-catch» for å bestemme brønnintegritetforhold. Tredjegrensesnittekko ble for denne metoden også registrert og ga rimelig nøyaktige målinger av tykkelsen på materialet bak stålet.

Behovet for sement evaluering vil øke i nær fremtid, og begrensningene i dagens verktøy er en årsak til bekymring, og videre forskning innen sement evaluering er etterspurt.

Acknowledgement

I would like to thank my co-supervisors Tonni Franke Johansen, Idar Larsen and Kristin Elisabeth Berg Pettersen at SINTEF for their great support and guidance during the thesis work, it was highly appreciated. A special thanks to all the good people working in the Formation Physics lab at SINTEF for helping me with some of the lab work.

A thanks should also be given to SINTEF Petroleum Research and NTNU for lending me the equipment enabling me to do the lab measurements and giving me my own office at SINTEF.

I would finally like to thank my supervisor Professor Rune Holt for setting me up with this thesis and supplying good source material as well as feedback. I would also like to thank him for giving me such freedom in my work.

K.H.

List of Figures

List of Tables

Contents

1 Introduction

In today's oil business, being able to accurately evaluate well integrity has never been more important. Wells are being drilled deeper, longer and under more challenging conditions than ever before. The life expectancy of a new oil well can often exceed 25-30 years. The need for good cement evaluation methods and tools is vital to achieve these long well life expectancies.

Cement evaluation is needed after every cementing operation to see if the goals of the job were met. However, the cement properties might change over time and old wells need re-evaluation. Plug and abandonment (P&A) is the name of the operation process where a well is prepared to be shut in and closed permanently. On the Norwegian Continental Shelf i.e., new drilling techniques and complex well paths allow fewer wells to drain a larger area of a reservoir. Many old well are becoming redundant and also many Norwegian oil and gas fields will go out of production in the coming years. Because of this, the demand for plug and abandonment services including cement evaluation will sky rocket. Being able to accurately measure the properties of media behind steel is a very pressing topic.

New cementing techniques and very low density cement sheaths have recently been developed. Foamed cement, for example, with its low acoustic impedance, poses a real challenge for the cement logging tools. These tools measure the attenuation of ultrasonic acoustic signals, and use this to calculate the impedance of the media behind the casing. Pulse-Echo and recently also leaky lamb wave measuring techniques are being used, and these will be explained in this thesis.

This thesis will present different ultrasonic cement evaluation tools and explain how they are used to evaluate well integrity. Extensive lab experiments have been conducted on a set-up by SINTEF Petroleum Research to test functionality, sensitivity and effectiveness of the the Pulse-Echo and leaky lamb wave measuring techniques, under various conditions.

The author has done previous unpublished work on a related subject in the fall of 2013, and chapter 2 and 3 of this thesis contain some of that work. Researcher Tonni F. Johansen at SINTEF has supplied a few ultrasonic computer simulations for this thesis, and these are published with his permission.

2 Cement Evaluation

When a cement job is evaluated it is determined whether the objectives of the job have been reached. The main objective of cementing the annulus between the formation and casing is to create zonal isolation between different formation layers, but there are other purposes too. [1]

2.1 Purpose

A primary cement sheath has various purposes depending on what casing string it supports. The main purpose of a cement job for the conductor casing is to prevent the formation from eroding. The cement stops the fluid circulation flow outside the casing and thereby prevents erosion. The surface casing, often set in depths that are related to water aquifers, needs to be cemented to seal and protect water formations. In the intermediate casing sting the cement is put in place to seal off abnormally pressured formations, shut off lost-circulation zones and to isolate weak formations. With the production string it is important to prevent upward migration of gas or fluids in the casing-formation annulus, so these strings are carefully cemented. Zonal isolation is important, and that is often one of the main things engineers look for in cement evaluation results. When remedial cementing is done, the objective is primarily to improve the quality of the existing cement job, casing leak repair and to seal of perforations. [1, 3]

Cement evaluation is done after a cement job to check if the objectives of the cementing job were met. It is difficult to successfully cement casing and liner and the operation requires proper planning. A good understanding and knowledge of the pressure mechanisms and well conditions during placement of the cement slurry is vital for making a good cement plan.

The causes of a bad cement job can be classified in two categories:

- Flow problems of mechanical origin
- Degradation of the cement slurry during the curing stage

Flow problems lead to incomplete mud removal in the cement annulus, and leave areas without cement. The cause of this can be poorly centralized casings, ineffective preflush, holes in the wellbore from wash-out and improper flow regime.[2]

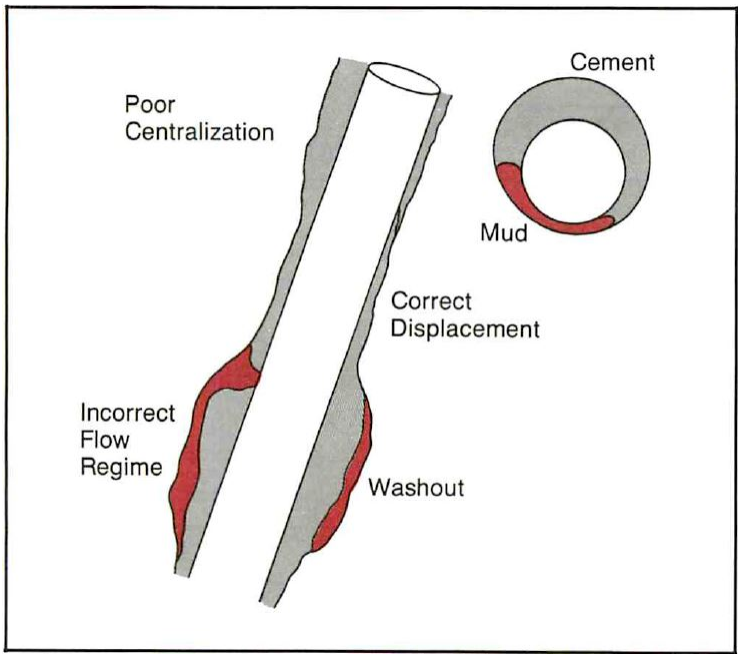

Figure 2.1: Cement slurry displacement problems [2]

2.2 Challenges

Field and laboratory tests have shown that differential pore pressure between the cement and the formation is the cause of many cement failures. During cement hydration, when the slurry loses water and shrinks, the pore pressure in the cement can become smaller than the formation pressure. The consequence of this can be cement pollution of formation fluid or inflow of gas. The latter, so called “gaseous” cement is unable to provide a proper seal for the formation gas. If gas is allowed to migrate within the slurry before the cement is set, the pore structure is partly destroyed. The gas will create a network of tubular pores and can lead to permeability as high

as 1 to 5 md.[2] Characterizing the cement properties outside of the casing is necessary to find out if some of these problems are present. Acoustic tools are used for this, but normal sonic instruments have a weakness; microannulus.

Microannulus

In this report a microannulus will be defined as a small fluid-filled gap between casing and cement. The gap can be as small as 1μm and up to a few hundred micrometers thick. These gaps are created when temperature or pressure changes occur during the setting of the cement. One example is when pressure in the casing is released before the cement is set, if 1000 psi is added to a 7-in. 23 lb/ft casing, the casing expands about 100μm. The effects of microannulus when it comes to sonic and ultrasonic tools will be discussed when the tools are explained. [6, 1]

3 | Ultrasonic Logging

Ultrasonic cement logging tools send out high frequency sound pulses from piezoelectric transmitters or transducers and measure the echo from the pulse either with the same transducer (pulse-echo) or at another receiver on the tool. The broadband pulse frequency is often between 200 – 700 kHz and makes a small area of the casing resonate through its thickness.[1] The transducers listen for this resonance or "ringing" and can by looking at the resonance amplitude attenuation calculate the acoustic impedance of the cement behind the casing. The higher the impedance, the better cement seal is present. Recently there is a new method being used, where the attenuation of flexural waves travelling through the casing is used to determine if a hydraulic seal is present. The theory behind this will be further explained in the report.

3.1 Brief History of Ultrasonic Tools

Ultrasonic logging tools have come a long way since they were first used for well logging in the 1960s. Zemanek and Caldwell (1969) were the first to use pulse-echo technology when they designed the "Borehole Televiewer" for imaging the borehole wall. Later the Cement Evaluation Tool (CET) was developed by Havira (1979; 1982) of Schlumberger. The CET tool uses 8 ultrasonic transducers spread around the circumference of the tool in a helical spiral at 45deg intervals. After this a lot of studies were conducted and field results were presented (Forelich et al. (1981), Dumont et al. (1984)) with models on how to interpret the results (Finlayson et al. (1984), Catala et al. (1984)). Two years later, in 1986, the Pulse Echo Tool (PET) was introduced by Sheives et al. of Gearhart Industries. Then in the 1990s some of the second generation ultrasonic tools still used today were introduced. In 1991 the Ultrasonic Imager (USI) by Hayman et al. for Schlumberger and in 1997 the Circumferential Acoustic Scanning Tool-Visualization (CAST-V)

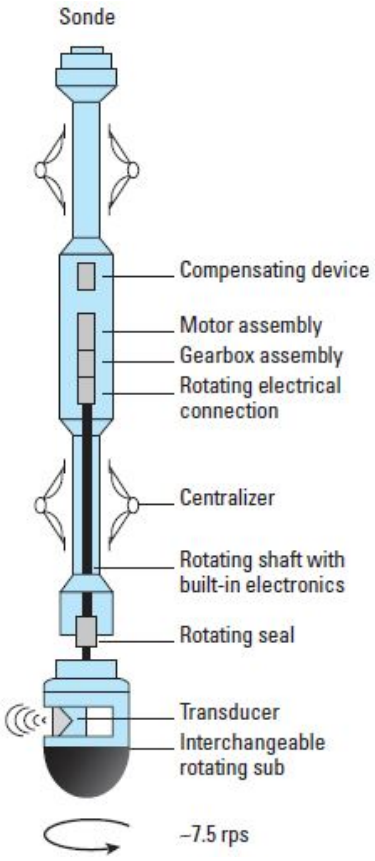

(a) USI tool[1]

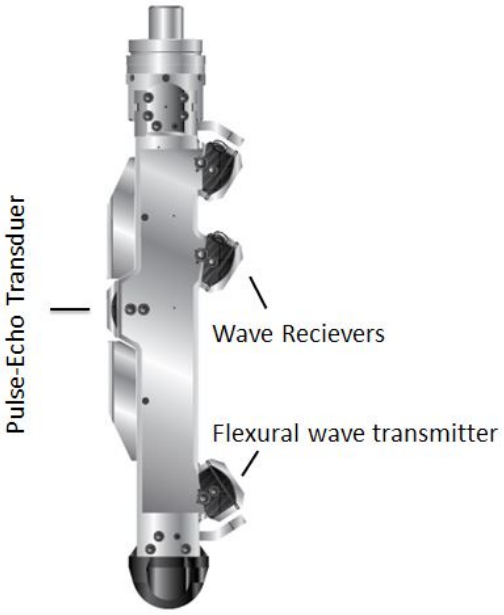

(b) Isolation Scanner Tool[16]

Figure 3.1: Ultrasonic evaluation tools

by Graham et al. for Halliburton were developed. These tools now use a rotating transducer to get greater accuracy by covering all angles of the circumference. Goodwin (1989) suggested one would use the absolute values of acoustic measurement, in addition to their character, to make it easier to distinguish between solids or fluids in the annulus. Statistical processing of ultrasonic images has since then become very common.[1] The latest within ultrasonic logging tools is the Isolation Scanner from Schlumberger first presented by Kuijk et al. (2005).[12] This scanner uses one ultrasonic transducer for pulse-echo measuring as well as one flexural wave transmitter and two receivers. The use of the flexural wave attenuation gives a better image of low-impedance cements.

3.2 Pulse-Echo Measuring

The main principle of pulse-echo evaluation is to send a high frequency pulse from a transducer normal to the casing wall and listen for the echo from this pulse. The frequency of the pulse can be between 200 to 700kHz and is chosen depending of the kind of steel in the casing, and fluid properties. The physics is explained by assuming a planar ultrasonic wave travelling perpendicular to a flat plate representing the casing. The pulse travels through the fluid inside the casing and hits the casing wall. When the contact is made most of the wave energy is reflected of the casing and travels back towards the transducer, but some energy is refracted (transmitted) through the casing wall. How much is reflected and how much is refracted is dependent on the contrast between the acoustic impedance of the fluid and the casing.[1] The specific acoustic impedance of a material is defined as the product of the material density and compressional velocity

$$Z = \rho \cdot v \tag{3.1}$$

where ρ is density and v is compressional velocity. The reflection coefficient (K_{ref}) is the fraction of how much acoustic pressure is reflected in a boundary between two media. K_{trans} is the transmission coefficient, and the formulas for them are as follows:

$$K_{ref} = (\frac{Z_2 - Z_1}{Z_2 + Z_1})^2 \tag{3.2}$$

and

$$K_{trans} = 1 - K_{ref} \tag{3.3}$$

Here Z_2 is the impedance of the material entered from the material with impedance Z_1. [1]

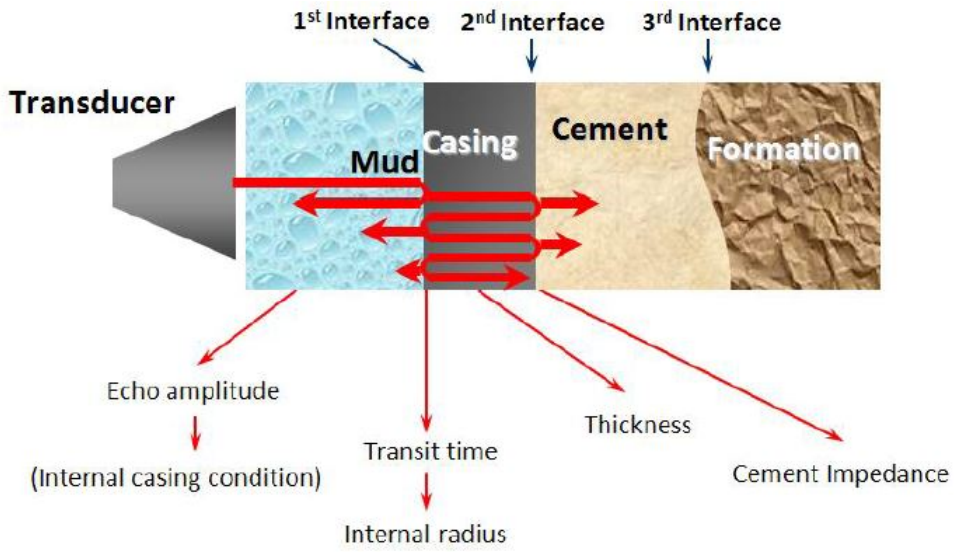

Figure 3.2: Illustration showing the compressional wave path and the information that can be gathered from it [5]

Figure 3.2 shows how the ultrasonic pulse travels further. The part of the ultrasonic signal that is transmitted into the casing will travel through the casing and hit the boundary between casing and cement. Again, some signal is reflected back inside the casing and some is transmitted into the cement. The pulse inside the pipe wall continues to bounce back and forth, losing energy into the annulus and the hole at every bounce. The casing resonates through its thickness mode. This process continues until the returned signal is too small to detect. K_{ref} inside the casing is negative, resulting in a series of echoes and the waveform received is exponentially decaying because of the excitation of energy within the casing wall.[1, 5]

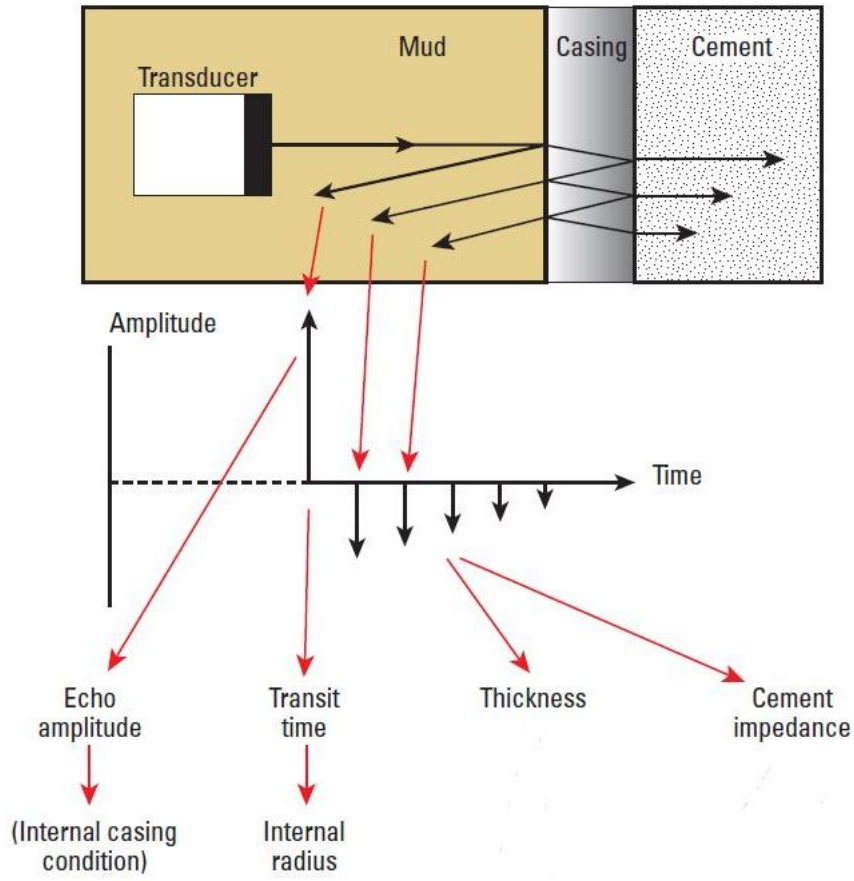

Figure 3.3: Illustration further showing how the interface reflections affect the signal [1]

An illustration of the information gained from the ultrasonic pulse-echo response can be seen in figure 3.3. The first big signal response is the initial reflection from the pulse striking the inner casing wall. By measuring the time difference from pulse transmission to reflection, one can calculate the internal radius of the pipe, and see if the tool is eccentered. The amplitude of this main echo can be used to give an indication of casing conditions like pipe rugosity and any presence of mud film. Next is the analysis of the weaker inverted pulses from the casing resonance ringing. Time separation between the pulses is equal to the go and return transit time in the casing. This can be used to calculate the casing thickness (h_{csg}) when the acoustic velocity in the steel (v_{steel}) is known.[1] The formula is

$$\Delta t = \frac{2h_{csg}}{v_{steel}} \tag{3.4}$$

From this travel time the resonant frequency of the casing (f_0) can also be found. The relation is

like this

$$f_0 = \frac{1}{\Delta t} = \frac{v_{steel}}{2h_{csg}} \tag{3.5}$$

It is important that the frequency used by the transducer match the resonant frequency of the casing. Earlier it is mentioned that the range of frequency used is from 200 to around 700kHz. This range is used because those frequencies correspond to the inherent thickness mode resonant frequency of casing used in petroleum wells, which usually range from 0.18 to 0.6 in. [4.57 to 15.24mm].[1] Hitting the right frequency, matching the resonant frequency of the casing, will result in greater amplitude in the oscillation of the casing.

When the casing vibrates it pushes against the cement, and the cement will therefore dampen the vibration. By looking at how much the signal is dampened for each time the pulse travels back and forth in the casing wall, it is possible to calculate the cement impedance. If the impedance of the media behind the casing is calculated as high, it is expected to be good dense cement there. If the impedance is low there might be fluid or less dense cement behind the casing. When these impedance data are interpreted, the selection of an acoustic impedance threshold between cement and liquid is set. This threshold is based on the acoustic impedance of the liquid that is expected to be behind the casing. Because of this, knowledge of the acoustic properties of the cement used is not very important. The threshold is used in the way that if the impedance measured is lower than the liquid/cement threshold, the zone is interpreted to be liquid, and vice versa.

The way the impedance is calculated from the resonance signal attenuation depends on the tool being used. The first generation tools, the CET and PET, compared the damping of the resonance signal in predetermined time windows. The USI tool processes the signal in the frequency domain, not the time domain like the CET and CET. In this report the newer USI tool measurement method will be explained.[1] The USI tool looks at roughly the first 7 cycles of resonance and uses group delay analysis. Group delay is a useful measure of time distortion, and is calculated by differentiating, with respect to frequency, the phase response versus frequency using discreet Fourier transform. The formula used is the rate of change of the total phase shift with respect to angular frequency

$$\tau = \frac{-d\varphi}{d\omega} \tag{3.6}$$

where $\varphi(\omega)$ is the phase spectrum and $\omega = 2\pi f$ is the angular frequency of the signal. This gives a spectrum in the frequency domain, and shows the pipe resonance as a dip. The bottom of this frequency spectrum dip is the value for the resonance f_0, and the width of the resonance $\frac{\Delta f}{f_0}$ depends on the cement impedance.[1]

3.3 Leaky Lamb Wave Measuring

Lamb waves are elastic waves propagating in solid plates. The English mathematician Horace Lamb published in 1917 the first study and description of waves of this type. He found them to be elastic waves whose particle motion lies in the plane that contains the direction of wave propagation and the plate normal (x and z plane). They include compressional and vertically polarized shear waves. By definition, the Lamb waves have no particle motion in the y-direction. The plate motion in the y-direction is caused by the vertically polarized shear waves. These have no motion in the x- or z- directions, and therefore complementary to the Lamb wave modes. As in Rayleigh waves which propagate along single free surfaces, the particle motion in Lamb waves is elliptical with its x and z components depending on the depth within the plate. [10, 19]

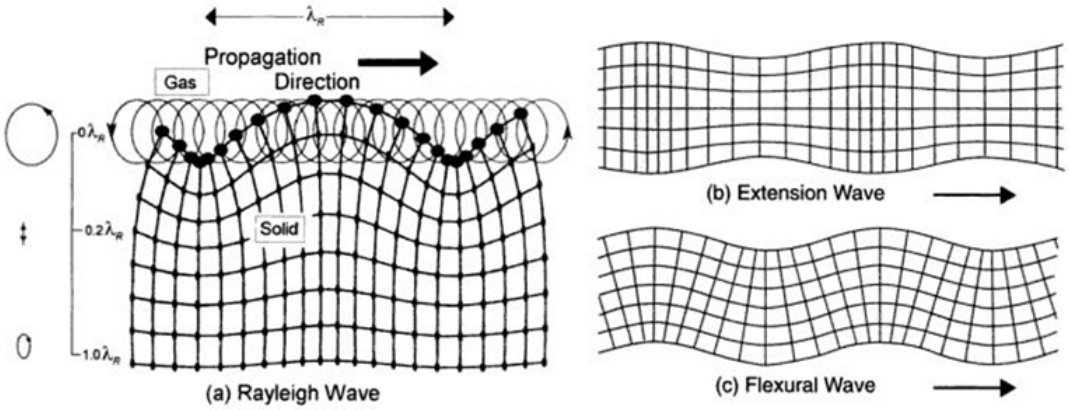

Figure 3.4: Illustration of particle displacement for the different waves [9]

When the frequency used becomes high enough (80 kHz or more), the ultrasonic pulse interacts with a small localized area of the casing. It is therefore possible and appropriate to look at this area as part of an infinitely unbounded steel plate. An infinite medium supports just two wave modes travelling at unique velocities; but plates support two infinite sets of Lamb

wave modes, whose velocities depend on the relationship between wavelength and plate thickness. [17] Lamb waves are elastic waves similar to longitudinal waves, but the particle motion is bounded by the plate surface causing a wave-guide effect.[13, 4]

3.3.1 Lamb Wave Modes

There are two modes that dominate the wave physics of a fluid-loaded plate in the frequency of interest. The first mode is the extensional mode, which is referred to as the lowest symmetric mode (zero mode) of the Lamb wave (designated s0). The second mode is the lowest antisymmetric mode of the Lamb wave, called the flexural mode (designated a0). These two modes have special properties in the way that they exist at all frequencies and they carry more energy than higher-order modes. As the frequency get higher, higher-order wave modes maker their appearance in addition to the zero-order modes. The higher order modes are "born" at a resonant frequency of the plate, each of these modes exists only above these certain frequencies which can be called their "nascent frequencies". None of the modes have any upper frequency limit. The zero-order modes have nascent frequency of zero, meaning that they exist over the entire frequency spectrum. These nascent frequencies can be pictured as the resonant frequencies for the compressional or shear waves, and are found by this formula:

$$f = \frac{nc}{2d} \tag{3.7}$$

Where n is any positive integer and d is plate thickness. The velocity c can here be either compressional or shear wave velocity, and each set of resulting resonances are alternately symmetrical and antisymmetric Lamb wave modes. For example, in a 12mm thick steel plate having compressional and shear velocities of 5890 m/s and 3260 m/s respectively, the nascent frequencies of the antisymmetric modes a1, a2 and a3 are 135 kHz, 271 kHz and 490 kHz respectively, while the nascent frequencies of the symmetric modes s1, s2 and s3 are 245 kHz, 407 kHz and 543 kHz respectively. Looking at the dispersion curves, which are graphs that show relationships between wave velocity and frequency in dispersive systems, it is possible to see which modes are present at a given frequency. [19, 4, 10]

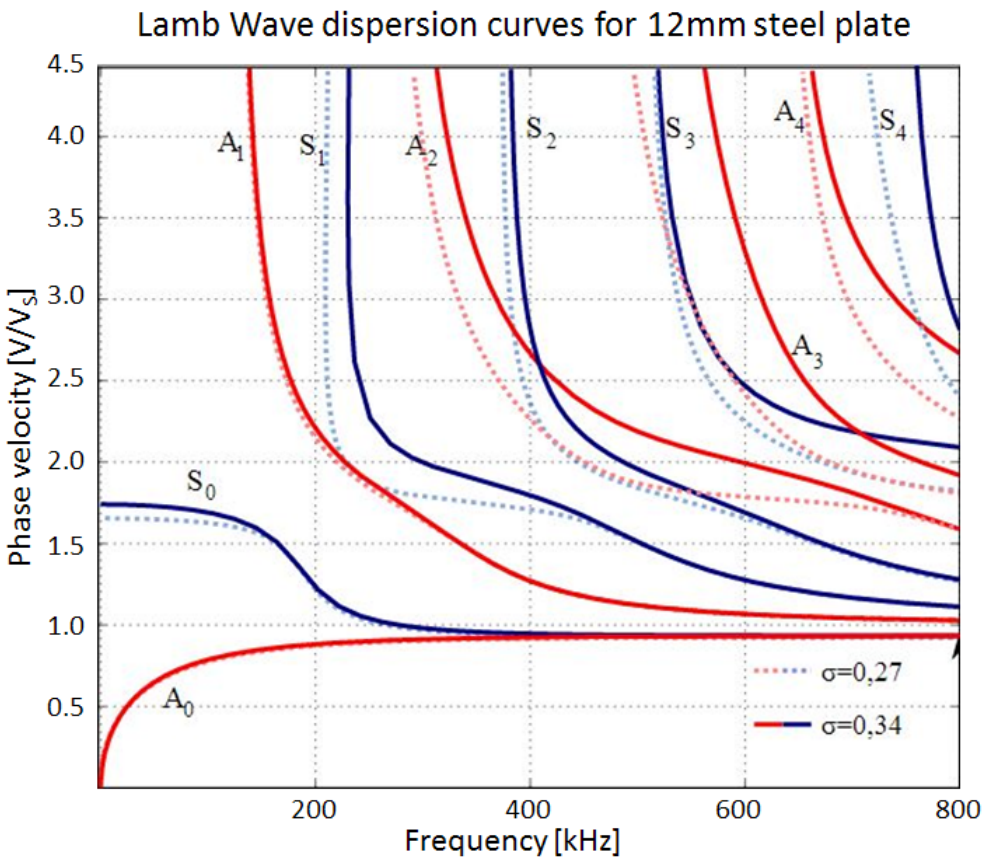

Figure 3.5: Lamp-wave dispersion curves for 12mm steel casing with two Poisson's ratios [19]

3.3.2 The Flexural Mode

The particle displacement in the extensional mode is symmetrical to the middle plane and mainly parallel to the plate. At low frequency this mode becomes the basis of traditional sonic cement logging tools. The flexural mode has a particle displacement antisymmetric to the middle plane and perpendicular particle motion with respect to the plate (see figure 3.4).[17]

Because the particle velocity and motion is perpendicular to the wave propagation, it is very dispersive. This creates a good connection between the surrounding media and the flexural wave has the properties to be a very good acoustic transmitter.[18] To better understand the following formulas presented the equations for longitudinal and shear velocity are given as

$$c_L = \sqrt{\frac{H}{\rho}} \tag{3.8}$$

and

$$c_S = \sqrt{\frac{\mu}{\rho}} \tag{3.9}$$

where ρ is density of the media, μ is shear modulus and H is the plate wave modulus defined as

$$E\frac{(1-\nu)}{1-\nu-2\nu^2} \tag{3.10}$$

where E is Young's modulus, and ν is the Poisson ration.[8] The differential equation that describes the particle velocity perpendicular to an isotropic plate surface is given as[18]

$$B\frac{\vartheta v_y}{\vartheta x^4} + m\frac{\vartheta^2 v_y}{\vartheta t^2} = 0 \tag{3.11}$$

Where B is the plate bending stiffness per unit of length and m is mass per plate unit. The wave number is calculated from this formula

$$k_F = \frac{\omega}{c_F} = \sqrt{\omega} \cdot \sqrt[4]{\frac{m}{B}} \tag{3.12}$$

Where the phase velocity c_F becomes

$$c_F = \sqrt{\omega} \cdot \sqrt[4]{\frac{B}{m}} \tag{3.13}$$

In formula (3.13) it is used that the wave solution is $v_y = \hat{v}_y \cdot e^{j(\omega t - k_n x)}$ to get k_F.

The wave being dispersive means that its velocities (phase and group velocities) are frequency dependent. The phase velocity is the velocity of peaks and troughs of a sinusoidal wave. The group velocity is the velocity of a packet of waves centered on a given frequency. A broadband pulse will change shape during the propagation, and wave components with a high frequency will tend to surpass the lower frequency components.[17] The equation with frequency taken to account is

$$c_F = \sqrt{\frac{\pi}{\sqrt{3}} c_L h f} \tag{3.14}$$

Here f is frequency and c_L is the longitudinal phase velocity. The formula is created by inserting

for m and B, where

$$m = p \cdot h \tag{3.15}$$

and

$$B = \frac{E}{1-\nu^2} \cdot I = \frac{E}{1-\nu^2} \cdot \frac{h^3}{12} \tag{3.16}$$

where I is the plate moment of inertia per unit of width. The expressions for wave number and phase velocity require that the plate is thin, and the wavelength must be larger than 6 times the plate thickness. For application with ultrasound and casing evaluation, for example, the wavelength might be 5,8 mm (in steel with 1MHz), therefore even shorter than normal casing thickness. To calculate the phase velocity of flexural wave in thicker plates Reissner-Mindlin (1951)[15, 11] thick-plate models are used. The phase velocity for these thick plates is[18]

$$\frac{1}{c'^3_F} = \frac{1}{c^3_F} + \frac{1}{\gamma^3 \cdot c^3_S} \tag{3.17}$$

With γ being a factor depending on the Poisson ratio ν after the following table:

ν	0.2	0.3	0.4	0.5
γ	0.689	0.841	0.919	0.955

Table 3.1: Factor for equation 3.17 from Poisson's ratio

In steel the Poisson ratio is approximately 3,0 and the phase velocity in steel plates at high frequency converges towards a constant value.

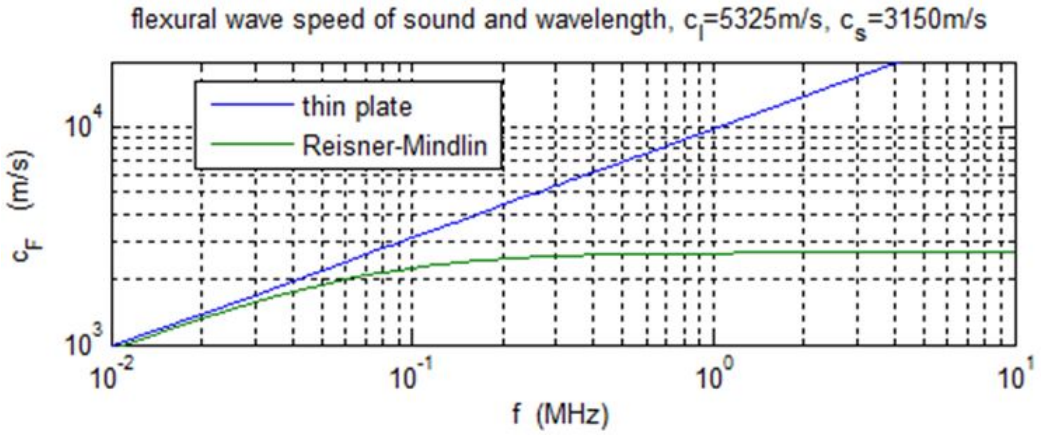

Figure 3.6: Flexural wave velocity vs. frequency for a 10 mm steel plate in a vacuum [5]

Figure 3.6 shows that above around 200 kHz the value converges to $\gamma * c_S$, which for steel will be around 84 percent of the shear wave velocity for a 10 mm thick steel.[18] The flexural group velocity will change as the phase velocity changes, but has a peculiar feature. It goes through a maximum at around 200 kHz and remains fairly constant at higher frequencies as well. This means that the frequency components of a broadband wave packet around this frequency will propagate at the same velocity, and therefore the wave packet will remain compact. This is important because the envelope of the flexural wave packet can be used to make accurate time of arrival and amplitude measurements.[17]

3.3.3 Exciting a Flexural Wave

To excite a flexural wave in the steel plate from the plane pressure wave from the piezoelectric fluid immersed transducer, the wave needs to hit the plate at a specific angle. The phase-matching angle, is the angle where the wave number of the water wave travelling along the plate matches the wave number of the flexural wave. This is dependent on the velocity of the fluid and the flexural wave, and is given by Snell's Law as

$$\sin\theta = \frac{v_f}{c_F} \tag{3.18}$$

where v_f is the sound velocity in the fluid around the transducer,c_F is the phase velocity of the flexural wave and θ is the approach angle measured with respect to casing normal. This angle is obviously dependent on fluid velocity and ranges from around 28 – 38 degrees, with typical casing fluid speeds of around 1250 - 1650 m/s. The faster the fluid speed, the smaller the approach.[17]

3.3.4 Flexural Wave Attenuation

The flexing motion of the casing is accompanied by attenuation of the flexural wave amplitude along its path. When it propagates it radiates energy into the inner and outer media. The flexural attenuation is dependent of the mechanical properties of both materials. The overall attenuation can be approximated to the sum of the attenuation due to the inner fluid and the attenuation due to the material outside the casing. For a fluid the attenuation is approximately

proportional to the acoustic impedance, but the situation is more complex when it comes to solid materials. Unlike a fluid, both compressional waves and shear waves can travel through a solid. So apart from density, acoustic wave propagation in a solid material is defined by the velocities of the compressional and shear wave. If the frequency of the flexural wave is 1 MHz and the casing thickness is 10 mm the flexural wave phase velocity will be 2750 m/s (3.6). In this case, to be able to radiate a compressional and/or shear wave into the cement the velocities of said waves in the cement must be less then 2750 m/s. Shear velocity in cement is always less than 2750 m/s and as a consequence, the shear wave is always radiated into the cement annulus, causing flexural wave attenuation. However, in good quality, high impedance cement, the compressional wave velocity might well be higher than the flexural phase velocity. In this case, the compressional wave cannot be radiated into the cement annulus (it is said to be supersonic compared to the flexural wave). This phenomenon has a decreasing effect on the attenuation, and gives an incorrect, too low, impedance reading (see figure 3.7).[17]

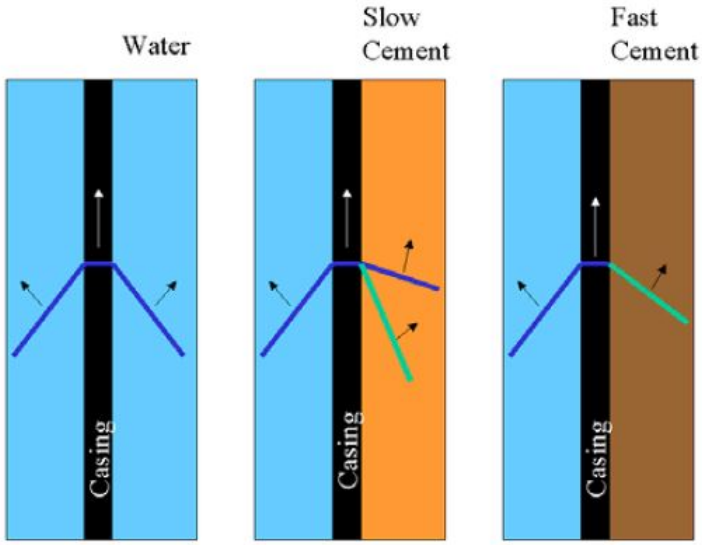

Figure 3.7: Radiation of flexural wave into cement with compressional wave velocity below and above flexural phase velocity. Blue is compressional wave front and green is shear wave front[17]

The impedance giving a higher compressional velocity is called the critical impedance, and on a plot of flexural attenuation versus acoustic impedance this point is called the Evanescence Point.

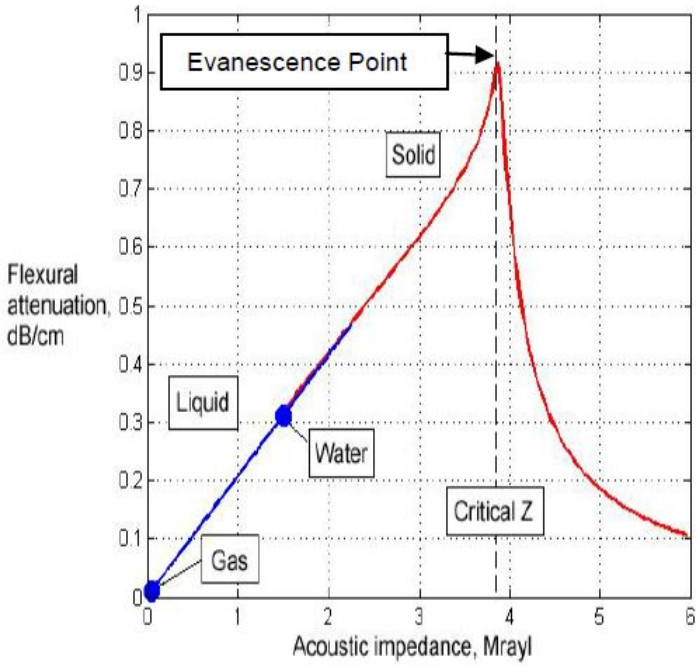

Figure 3.8: Flexural attenuation vs. acoustic impedance plot showing the effect of the evanescence point[5]

Below the critical impedance the attenuation increases linearly with material impedance, however, above this limit the attenuation drops rapidly to small values. A given attenuation then corresponds to two values of impedance, typically high impedance cement or a liquid. Flexural attenuation alone can therefore not be used to discriminate between liquid and good cement, and needs to be combined with another measurement, such as casing resonance pulse-echo technique.[17]

The effect of microannulus (described in section 2.2) on attenuation measurements with flexural waves is not very significant. For cement impedances lower than the critical impedance, there is a 15% reduction in attenuation as soon as the casing and cement are debonded. This is half the effect experienced with pulse-echo, which is about 30% reduction. The reduction is unaffected at 15% for microannulus width up to around 250 μm. Above the critical impedance, a large increase in attenuation is observed as the cement is debonded. The attenuation increases linearly with cement impedance, seemingly unaffected up to a microannulus width of 250 μm. This last effect is notably different from the pulse-echo technique and reduces the possible confusion between good cement with microannulus and mud.[17]

3.3.5 Third Interface Echo

As explained above, the flexural Lamb-wave pulse radiates or "leaks" energy out of both sides of the plate as it vibrates across the casing. The pulse being radiated into the casing-formation annulus will travel through the annulus media and reflect back when hitting the formation-(annulus media) interface. When this third interface echo (TIE) again hits the casing, it creates a new flexural wave in the steel, which radiates back into the annulus of the casing. Because it travels through the annulus, the echo from the formation interface can carry information on well geometry, annulus material, as well as formation acoustic contrast with the annulus media.

Depending on what type of media is present in the annulus, the annulus wave may result in different echoes. With fluid in the annulus, only pressure waves can propagate yielding only one type of TIE. With dense, fast cement as mention in section 3.3.4 only shear waves will propagate giving a slight different wave path than the compressional wave. The shear wave will of course still convert to a pressure wave in the casing fluid. Slow cement on the other hand will show an echo from; the compressional wave, shear wave and also echoes from waves that have partially converted from pressure to shear waves (and vice versa) upon reflection at the formation interface. The radiated wave pulse from the initial flexural wave will also continue to reflect back and forth within the casing-formation annulus, giving multiple TIE, each a little weaker than the last.

There are many factors affecting the amplitude of the TIE, and it may not always be detectable. For the TIE to reach the receiver in the casing annulus the reflected pulse needs to hit the casing with the correct flexural wave inducing angle mentioned in section 3.3.3. If the formation geometry reflects the wave back with a different angle than the incident angle, no flexural wave will be created and a lot less to no energy is transferred through the casing. Casing eccentering will also cause this problem, in the direction where the casing wall and formation wall is not parallel.

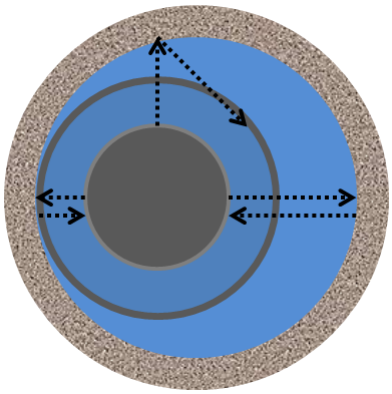

Figure 3.9: TIE measuring problem with casing eccentering in the borehole

Attenuation in the annulus material can also cause problems in detecting the TIE. Water and uncontaminated set cement usually have low attenuation, but heavy muds and unset/foamed cement might have high attenuation. Furthermore, if the impedance contrast between the formation and the annulus media is low the reflection will be low, resulting in a weak TIE. Shale and lightweight cement is an example media with low impedance contrast, and in these areas the TIE will be low. If the flexural measuring method is used in a double string, this would naturally result in a strong TIE, because of the high contrast. Large distance between the casing and formation can also be a problem, not only because of increased attenuation but because the echo might arrive outside of the recorded time window.

4 | Ultrasonic Lab Experiment

This ultrasonic measurement experiment was conducted at the Laboratory of Formation Physics at SINTEF Petroleum Research in Trondheim, Norway. The experiment was a continuation of work done by the author during the fall of 2013. The purpose of the experiment was to use the SINTEF prototype "Behind Casing Logging Set-up" or "BeCaLoS" to perform ultrasonic measurements on media behind steel casing using the pulse-echo and pitch-catch technique.

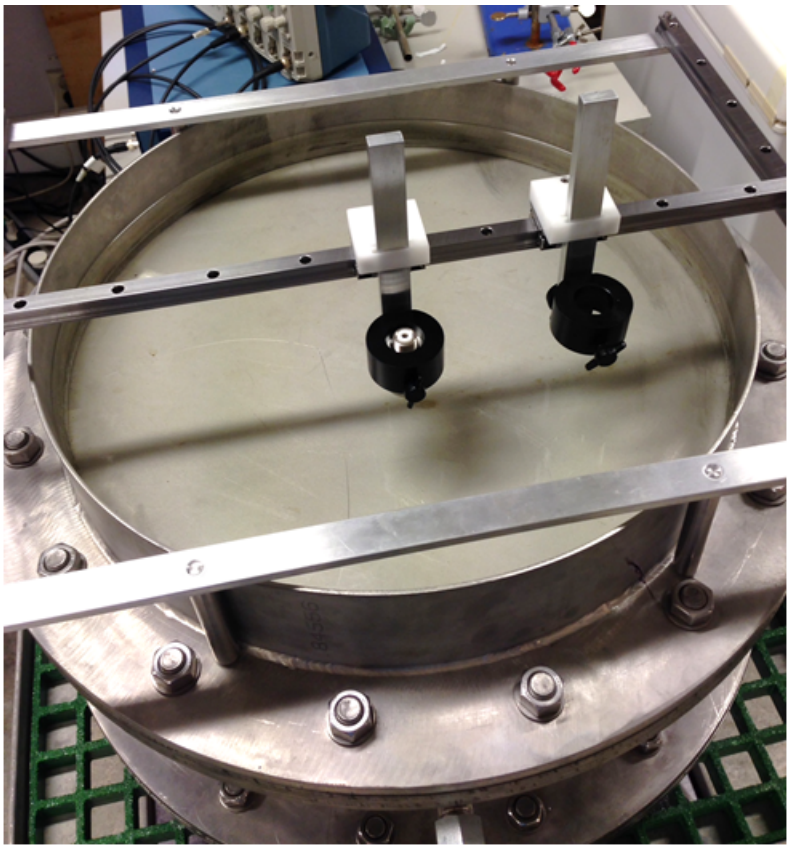

Figure 4.1: The BeCaLoS steel tank and transducer holder array

The experiment tests the different measuring techniques with special focus on flexural LLW and

TIE measurements. The techniques are tested using different frequency transducers and with air, water, mud and cement as annulus media. An artificial sandstone was cast to be used to represent the formation during the measurements. The next sections will explain the experiment equipment and set-up in more detail.

4.1 Set-Up

All the measurements were done using the BeCaLoS. The BeCaLoS is a stainless steel cylinder tank with a transducer holder system on top, see figure 4.1. The BeCaLoS was designed by SINTEF to enable easy ultrasonic measurement using pitch-catch and pulse-echo with varying content inside the tank. The tank plate is circular with a diameter of 500mm and a plate thickness of 12.1mm, and the steel cylinder underneath has a length of 200mm with the same diameter. The plate is connected to the steel cylinder with bolts and has an O-ring seal to keep the content of the tank from leaking out. On top of the top plate there is an open cylinder with an O-ring seal as well. Near the top of the cylinder, on opposite sides, there are two pipe openings with valves mounted which are used for injecting water/mud/cement. There is also a small hole in the top plate close to one of the pipe openings; this is used to let air escape during injection. The transducer-holder array is basically five thin steel rails, four of which are mounted in a rectangle, with the fifth connected to two of the sides with ball bearing slider-holders. This fifth steel rail going across has two ball-bearing holders with a steel rod going through it with connection for a transducer-holder on the bottom. The transducer-holder can also be tilted. This array allows the user to change the position of the transducer in the x-, y-, and z-direction as well as tilt the transducer with a specific angle. Figure 4.2, shows the inside of the tank. From the bottom of the tank coarse sand is used as a filler, to elevate the artificial sandstone. The tank content planned was to have 130mm of coarse sand, then 50mm of artificial sandstone allowing for 20mm annulus between the steel plate and “formation”.

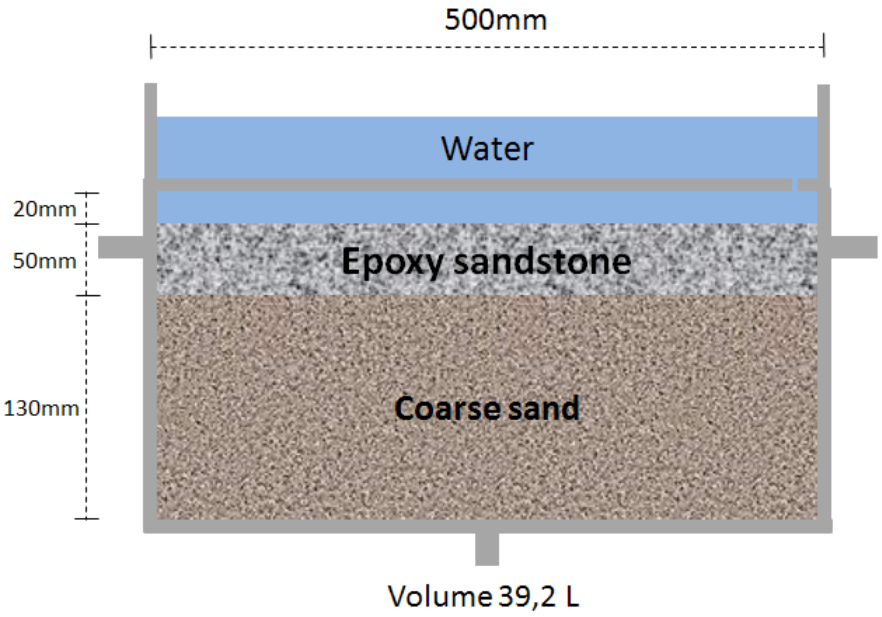

Figure 4.2: Illustration of the measurements and content of the BeCaLoS

4.2 Equipment

The instrument used to do the measurements were Panametrics piezoelectric ultrasonic immersion transducers from Olympus Inspection and Measuring Systems (IMS). The transducer is a single element longitudinal wave transducer with a ¼ wavelength layer acoustically matched with water.[14] The transducers had a frequency of 1MHz and 500kHz with a nominal element size of 25.4mm (1 in.) and 38.1mm (1.5 in.) respectively.

Figure 4.3: The type of transducer used for doing the measurements (not the specific one used in the experiment)[14]

An ultrasonic pulser-receiver, also from Olympus IMS was used to send a pulse with the transducers. To get the signal reading from the transducers a Digital Phosphor Oscilloscope (DPO) 3000-series from Tektronix was used. The oscilloscope was controlled by a computer running National Instruments LabVIEW Signal Express Tektronix Edition and the signal readings were recorded on the computer. To interpret the signal recordings, a MATLAB script developed by SINTEF Petroleumsforskning called Matlab Ultrasonic Analyser (MUSA) was used.

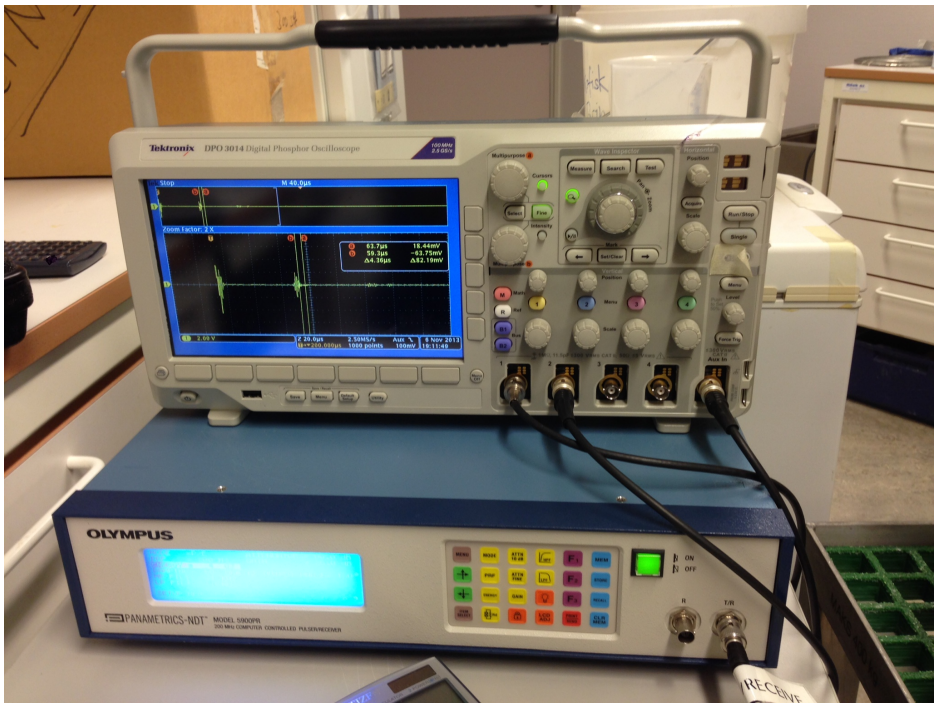

Figure 4.4: Image of the oscilloscope and pulser-receiver[14]

4.3 Execution

4.3.1 Artificial Sandstone & Annulus Media Injection

The need for a flat even surface with a known impedance and a specific size led to the decision to create a sandstone artificially. The sandstone was created with fine-grained sand cemented together using epoxy. This method has been tested before by R. M. Holt et al. in 2003 [7] using glass beads cemented together with epoxy to create a rock-like material. A number of different test-sandstones were created with varying sand/epoxy ratio, and they were all tested for compressional sound velocity and density, water saturated and dry.

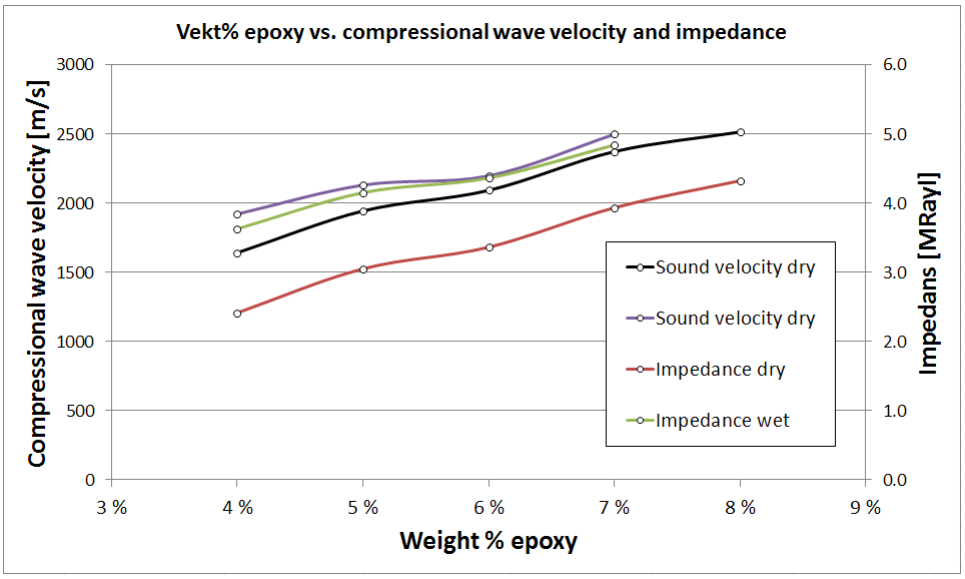

Figure 4.5: Impedance and p-velocity values vs. epoxy content in artificial sandstone

Figure 4.5 shows the ratios tested, and 7 weight % epoxy was selected to be used inside the BeCaLoS, to give a good impedance contrast between water and formation, and to have similar acoustic properties to that of sandstone. The epoxy glue was mixed together with the sand until the glue evenly covered all the sand gains. A masonry trowel was used to spread the glued sand out evenly and flat inside the BeCaLoS steel cylinder where it was left to harden for 24 hours.

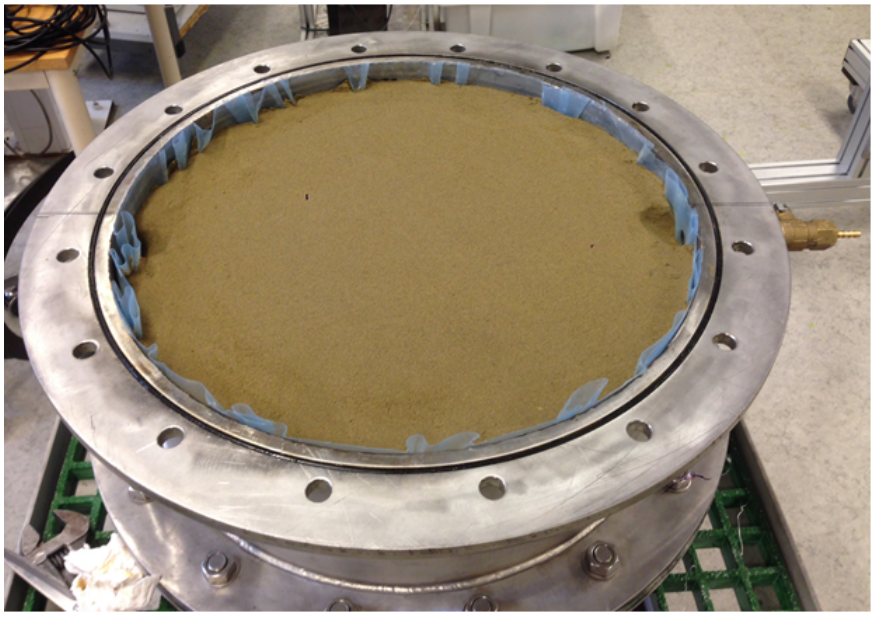

Figure 4.6: The artificial sandstone inside the BeCaLoS

The method used to change the annulus media once the stone was set and the state of the BeCaLoS during the different measurements were as follows:

Air

The set-up with air as the annulus media was done right after the artificial sandstone had set. The stone was dry and both side-valves on the BeCaLoS were open. The hole in the steel plate was closed, so no water would leak through from the open cylinder above. The whole BeCaLoS was also tilted 8 degrees while the measurements where done. This is to minimize the amount signal interference from waves that only propagate between the steel and the water. These signals are of no great interests and only make interpretation of the plate wave signal more difficult.

Water

The annulus thickness was found by measuring the distance from the steel plate to the sandstone. The distance was found to be 22.5mm. Degassed water was injected into the annulus by using a pressurized container and connecting this to one of the side valves via. a pressure hose. The BeCaLoS is tilted upwards in the direction of the hole in the plate, so that when water flows through a small tube connected to the hole the tank must be completely full. Because of the tilt all potential air bubbles will find their way up thought this hole. The BeCaLoS was set with water for half a day to let all air escape and the artificial sandstone to be saturated with water before any measurements were performed. The measurement is also done while the BeCaLoS is tilted and compressed air is blown over the water to create waves when the readings are done. This is again done to remove the signal from the water-waves travelling between the plate and water-air boundary.

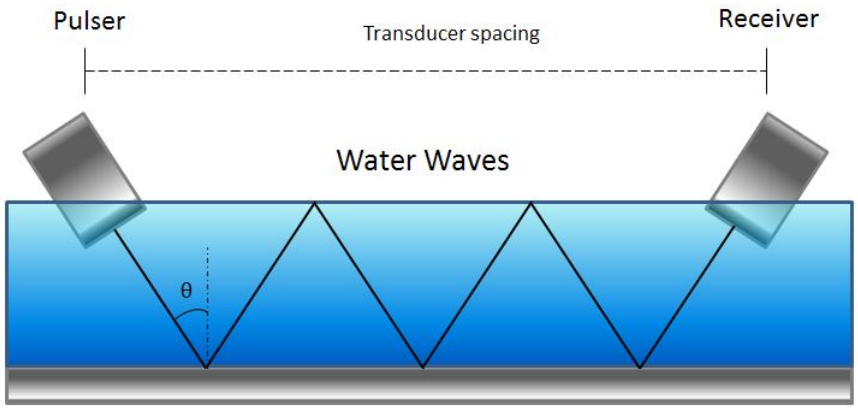

Figure 4.7: Illustration showing the water wave propagation with the P-C set-up

Mud

After the BeCaLoS had been drained of water, water-based mud was injected into the annulus. This was done in the same way as the water injection. The mud has a density of $1.3 g/cm^3$ and a compressional wave velocity of $1418 m/s$ giving an impedance of 1.84 MRayls.

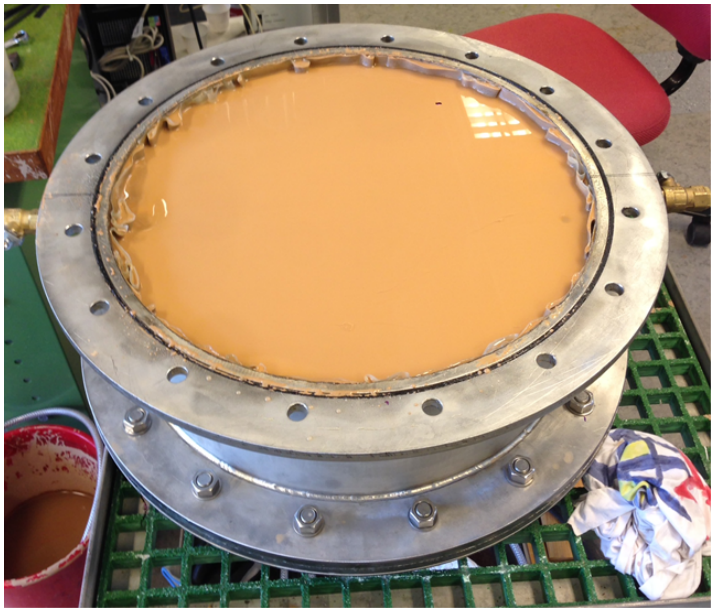

Figure 4.8: View of the annulus after mud measurements had been performed

Cement

Before cement could be injected into the annulus, the mud was drained and the BeCaLoS flushed with water. The artificial sandstone was cut and lifted out of the tank and mud

that had settled on the stone was removed. The coarse sand was removed and new sand was put in. The cleaned sandstone was put back in place and plastic wrapping was put in place around the cylinder walls to prevent the cement from getting stuck inside the BeCaLoS. The distance between the steel plate and the sandstone was again measured and found to now be 24mm. Class G cement with a water/cement weight ratio of 0.45 was mixed up and injected into the side-valve the same way as the mud and water, but higher pressure was needed from the container. The cement was left to set for 24 hours before measurements were performed. A small sample of the cement was cast and found the density to be $1.9 g/cm^3$ and the compressional wave velocity to be $2840 m/s$ with the corresponding impedance of 5.41 MRayls.

4.3.2 Pulse-Echo

The Pulse-Echo measurements were done on the BeCaLoS for each new content inside the tank; air, water, mud and cement. This measurement was performed by placing one transducer right at the center of the top steel plate with the position 300x150mm. The water column over the steel plate was 50mm and the transducer was held in place exactly 40mm above the steel plate. The signal response to pulse-echo readings is strongest when the transducer is perfectly parallel to the steel plate, and it is very sensitive to only the slightest offset. To be sure to get the strongest possible reading the oscilloscope was set to show a continuous signal reading and the transducer was adjusted until the point of strongest signal amplitude was found. The transducer was set to this position where the incident is believed to be perpendicular to the plate surface. A pulse was triggered with energy of 1 μJ and 0 dB attenuation, and 32uJ and 0 dB attenuation for the 1MHz and 500kHz transducers respectively. The oscilloscope took a reading of 1 million points. The signal was inspected using the display on the oscilloscope to check for signal cut off. If the entire signal was complete without any cut-off's the signal data was stored on the computer. There was also done a signal reading of 32uJ energy for the 1MHz transducer to better be able to see a possible TIE from the pulse-echo measurement.

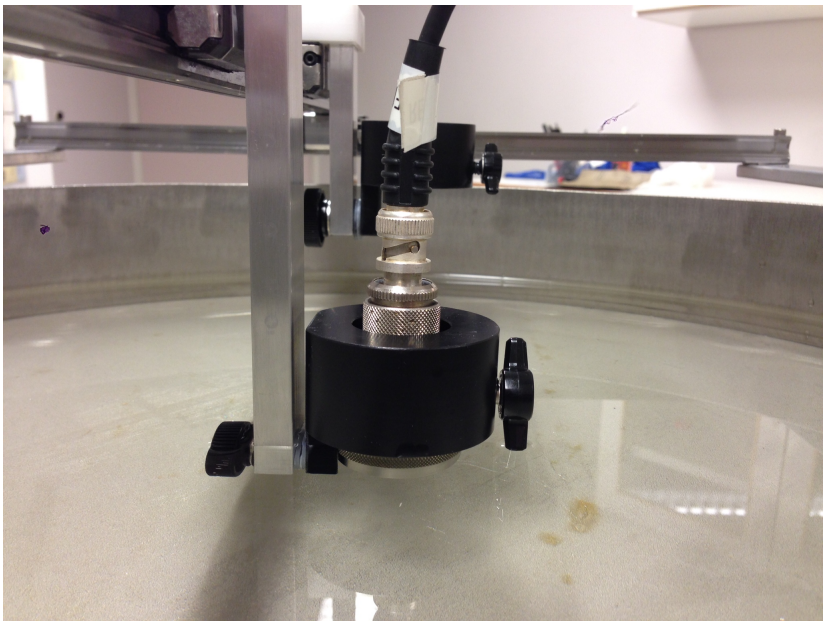

Figure 4.9: Image showing the transducer-holder and set-up when doing the Pulse-Echo measurements

4.3.3 Pitch-Catch

The pitch-catch technique involves using two transducers, one acting as a transmitter and the other as a receiver. Two pairs of transducers with identical specifications were used to perform the measurements. Figure 4.10 shows how the set-up was done, with both transducer element surfaces submerged in water.

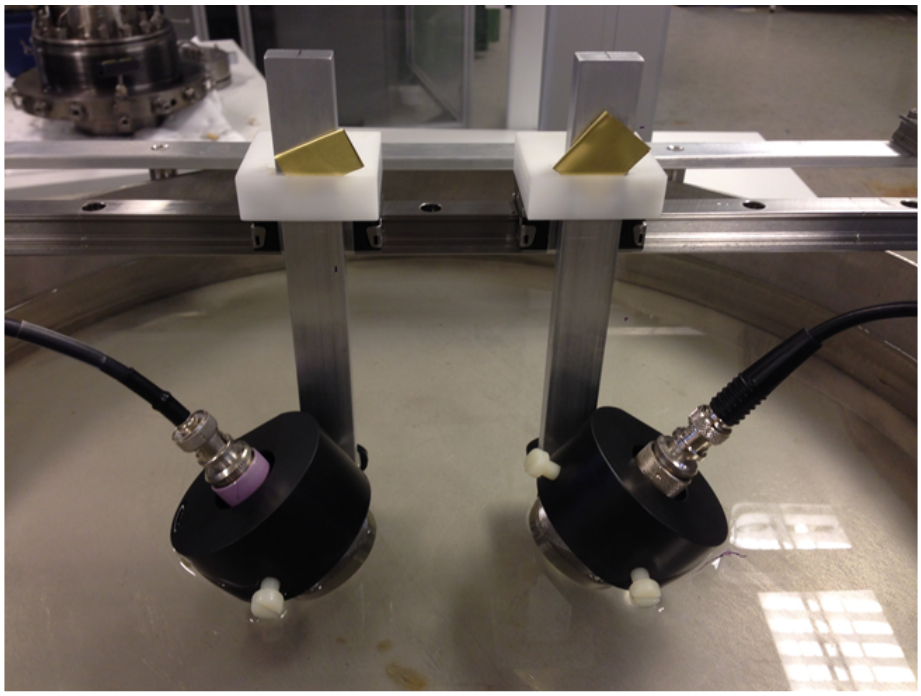

Figure 4.10: Pitch-Catch transducer holder set-up

The purpose of using the pitch-catch technique in this case is to measure attenuation and travel-time of the plate flexural wave. This wave is created using a specific incident angle as explained in section 3.3.4 and the incident angle needed to excite a flexural wave is given by equation 3.18, and is as follows:

$$\sin\theta = \frac{v_f}{c_F} \Rightarrow \theta = \arcsin\frac{1490 m/s}{2750 m/s} = 33\,\text{deg}$$

where the flexural phase velocity is taken from figure 3.6. During the experiment however, it was found that the angle that gave the highest signal reading was 30deg, this is discussed further in chapter 6. The transducers were therefore held at an incident angle of 30deg, with the receiver mirrored to face the pressure pulse from the flexural wave. The angle of the transducers is measured using an application on a smart phone utilizing the internal high sensitivity accelerometer and 6-axis gyroscope. Measurements were taken with varying transmitter-receiver distance to be able to see the attenuation of the plate wave. The distances used, measured from the center of each transducer element, were 60, 70, 80, 90, 100, 110, 125, 150, 175, 200, 225 and 250mm. The distance from the center of the transducer element to the steel plate was 40mm. For the 1 MHz transducer a pulse with 1μJ energy was used. The 500kHz transducer had to use 4 μJ to be able to see the signal at the largest distances. A 32 μJ energy signal, the highest possible from

the amplifier, was also recorded for each distance and frequency. This was done to make sure a possible TIE was measured, and not lost because of too weak a signal.

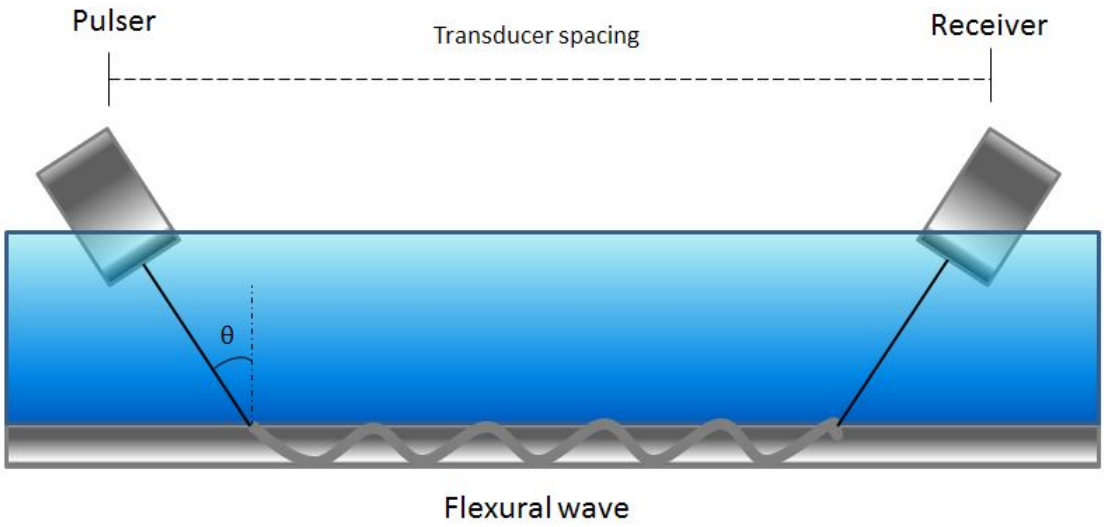

Figure 4.11: Illustration showing the flexural wave set-up and wave path

5 | Results

In this chapter the results from the lab experiment, including amplitude data, travel time data and attenuation data, will be presented. There will be some analysis of the results, but most of this will be done in chapter 6 Discussion.

5.1 Angle measurement & mode analysis

An angle analysis was done to find the optimal incident angle to give the highest amplitude plate wave. This was done by varying the angle of the transducer and receiver. The distance between the two was kept constant at 175mm. The measurement was done with the 500kHz transducers using 32 μJ pulse energy.

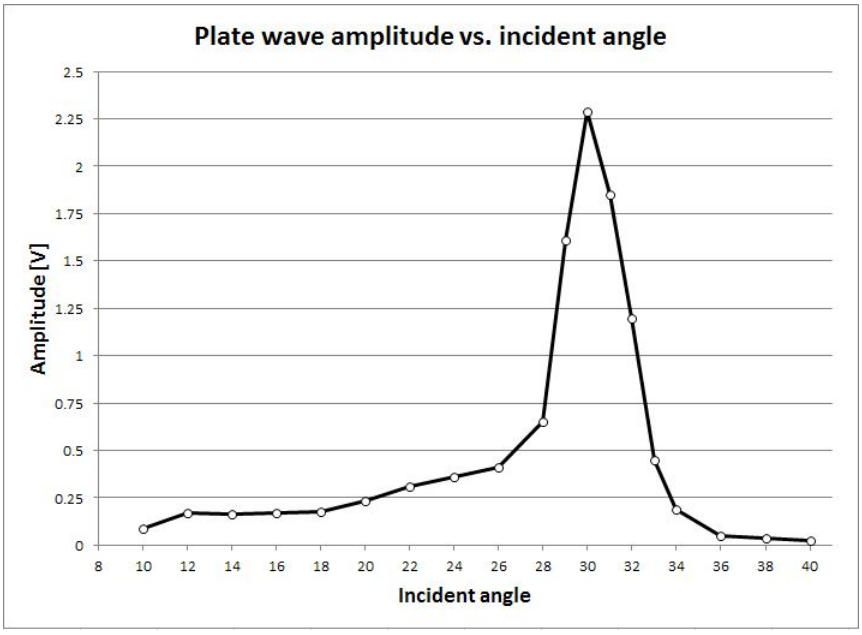

Figure 5.1: Plate wave amplitude vs. incident angle of the transducer pulse

From figure 5.1 it is clear that the plate wave has the strongest amplitude when the incident angle is around 30 degrees. It is also evident that the amplitude is quickly reduced to low levels as soon as the angle deviates from the optimal 30 deg. The interval for which there is any significant amplitude is 28-33 degrees. Scientist Tonni F. Johansen (SINTEF Acoustics, 2014) used COMSOL Multiphysics to look at what angles gave the most transmission and reflection through a 12mm thick steel plate at 500kHz. The following figure 5.2 shows the simulation results.

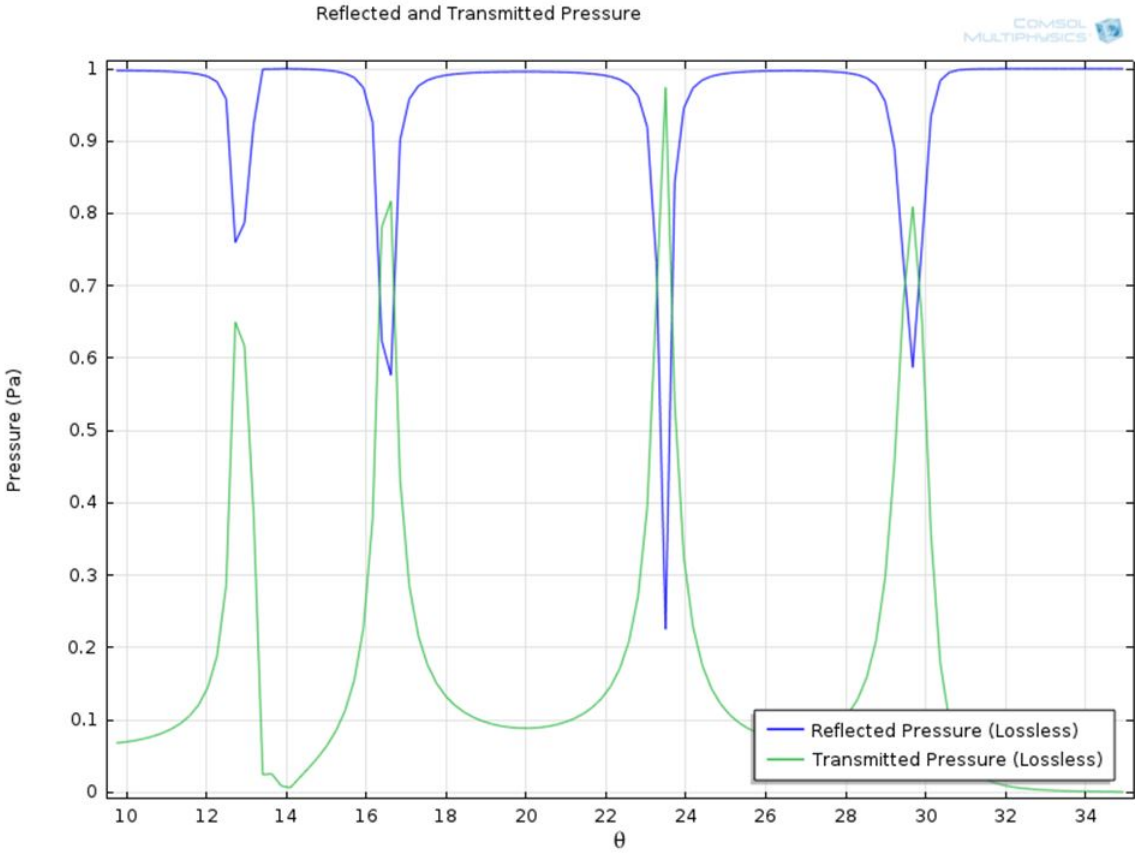

Figure 5.2: COMSOL Multiphysics simulation of transmitted pressure through a 12mm steel pate vs. wave incident angle courtesy of Tonni F. Johansen

The simulations indicate 4 possible angles that give good transmitted pressure. 13, 16.5, 23.5 and 29.5 seem to be angles of interest, all with very narrow transmission windows. The flexural mode is the mode which transmits the most energy into the surrounding media. Energy might well be transmitted into the steel plate at certain angles, but only the flexural mode will show high amplitude readings at the receiver end. Further simulations were done in COMSOL by Tonni F. Johansen to look for what modes were present in the steel using the different incident

angles. Below these results are compared to the actual waveform recorded in the lab experiment.

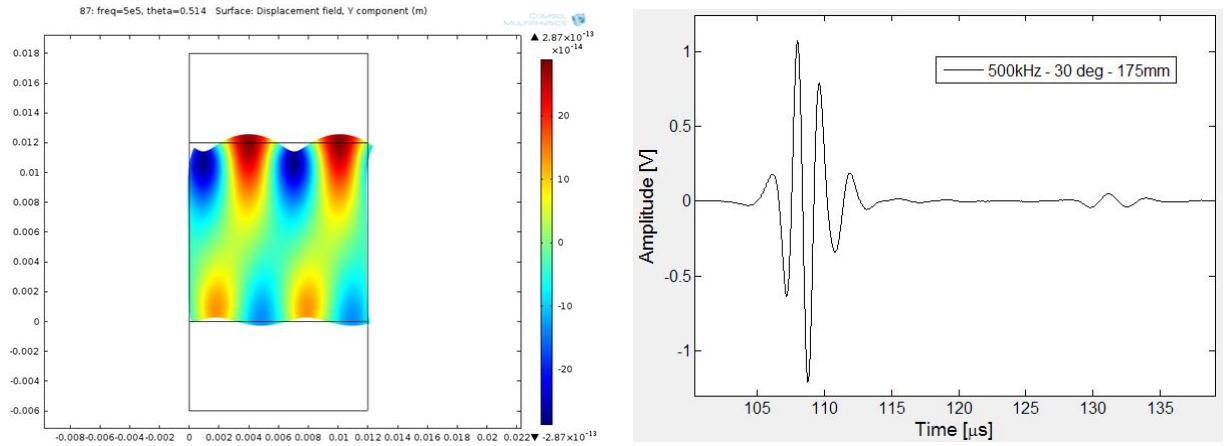

(a) COMSOL simulation of plate bending

(b) Waveform recorded in lab

Figure 5.3: Comparison of simulation of plate bending and waveform recorded at 30 deg. incident angle

In figure 5.3a the plate bending motion seems to be a cross between extensional (symmetric) and flexural (antisymmetric). The peak at the top of the plate corresponds to the middle between a peak and a trough on the bottom of the plate. The waveform in figure 5.3b shows a strong compact wave and the TIE wave is also recorded at around 130 μs. The fact that the TIE is present gives an indication that a good amount of energy is transmitted on the other side of the steel plate which is characteristic of a flexural wave. The wave peak to peak amplitude is over 2V and the pulse only lasts about 8 μs. At 24 degrees incident angle in figure 5.4a the simulation shows a higher-order flexural bending of the plate. The first-order antisymmetric mode might be excited at this angle. The waveform recorded shows a much longer, weaker amplitude pulse. This pulse is around 0.4V peak to peak amplitude and lasts about 25 μs. At the angle of 16 degrees the simulation in figure 5.5a seem to show a higher order extensional mode. This looks to be the second-order symmetric mode. Much of wave energy is lost to inner vibrations of the plate, and there is less bending. Figure 5.5b also shows even weaker peak to peak amplitude of about 0.15 V and a very long pulse. The pulse lasts about 40 μs and looks to have some areas with stronger amplitude than others. The pulse right after the 130 μs mark might be a TIE, but it is hard to tell. The final comparison at 12 deg incident angle show a more indistinguishable wave bending motion. The figure 5.6a seem to show a weak extensional mode of a higher order.

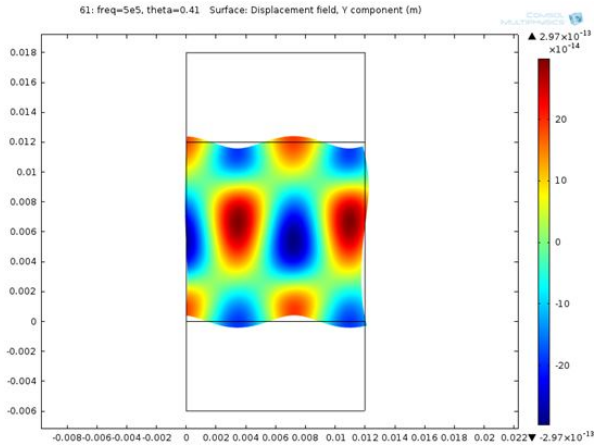

(a) COMSOL simulation of plate bending

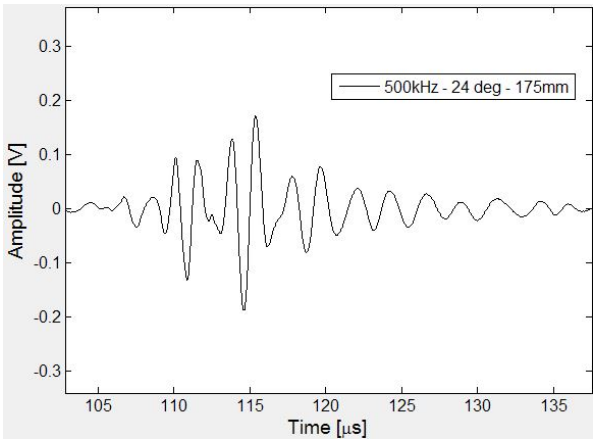

(b) Waveform recorded in lab

Figure 5.4: Comparison of simulation of plate bending and waveform recorded at 24 deg. incident angle

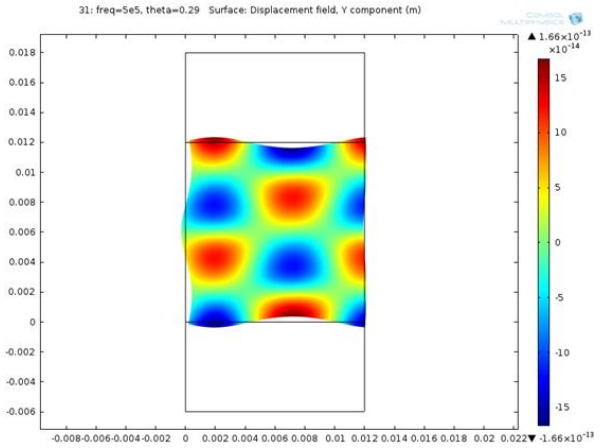

(a) COMSOL simulation of plate bending

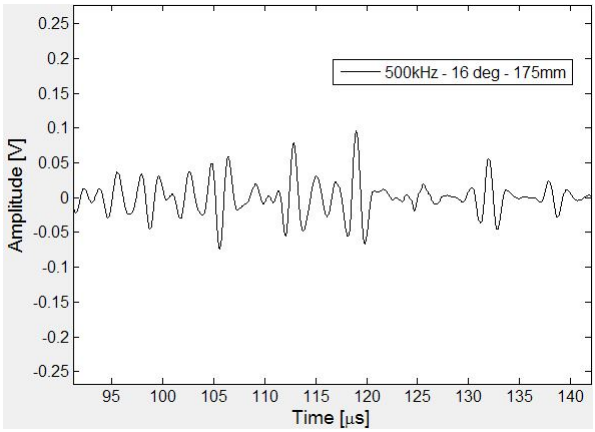

(b) Waveform recorded in lab

Figure 5.5: Comparison of simulation of plate bending and waveform recorded at 16 deg. incident angle

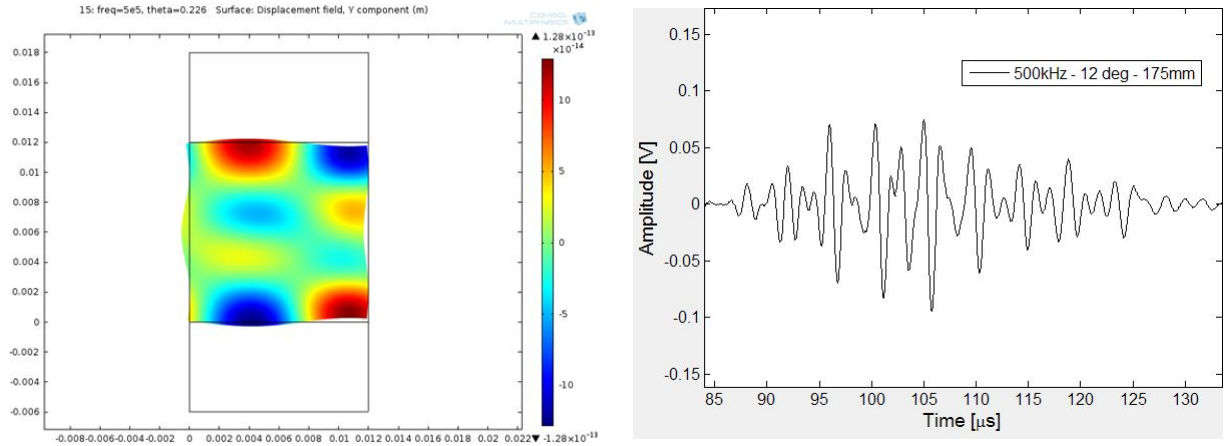

(a) COMSOL simulation of plate bending

(b) Waveform recorded in lab

Figure 5.6: Comparison of simulation of plate bending and waveform recorded at 12 deg. incident angle

The waveform recorded in figure 5.6b is a long pulse lasting around 40 μs and with a more even spread of peaks and troughs with a maximum amplitude of about 0.16V.

From this analysis it is possible to say with certainty that 30 degrees incident angle gives the highest energy transmission from the plate. The other angles indicated by the simulation to give good energy transmission gave other higher-order modes and were not suitable for Pitch-Catch measurements. All the pitch-catch measurements were therefore done with 30 degree incident angle.

5.2 Pulse-Echo

In this section pulse-echo measurements will be examined and analysed. Waveforms are shown, steel plate thickness, - resonance and attenuation is calculated.

The pulse-echo readings gave as expected a strong first pulse followed by a series of lower amplitude pulses from the resonance ringing of the steel. The pulse-echo reading with air as the annulus medium naturally gave the strongest resonance ringing, and figure 5.7 shows the waveform recorded with a 1MHz pulse.

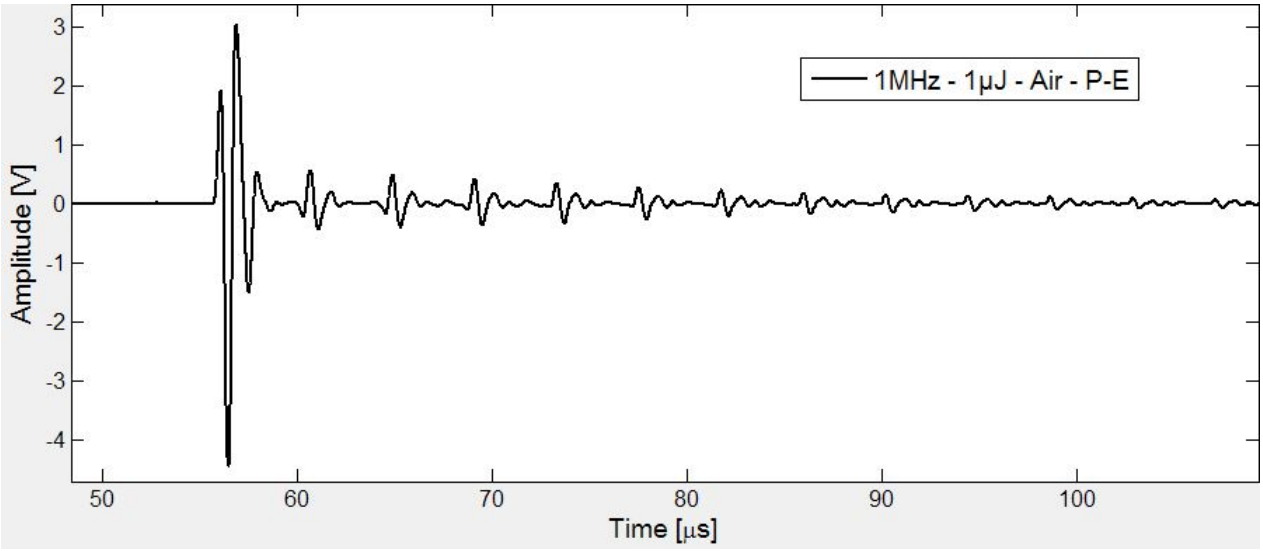

Figure 5.7: Graph showing the signal measured with pulse-echo through water, steel and air

Figure 5.7 shows a first strong pulse after 56 μs, which is the initial reflection of the compressional wave pulse hitting the steel plate. All the following pulses are signal which is reflected from the pressure wave travelling back and forth through the thickness of the steel plate. Even at the lowest signal energy 1 μJ the initial reflection is over 7.4 V in amplitude. This is because most of the signal is reflected back from the high impedance contrast between water and steel. All the signals recorded, whether it was with 1MHz, 500kHz, air or cement, this waveform pattern was observed, with one strong first pulse and several weaker pulses following.

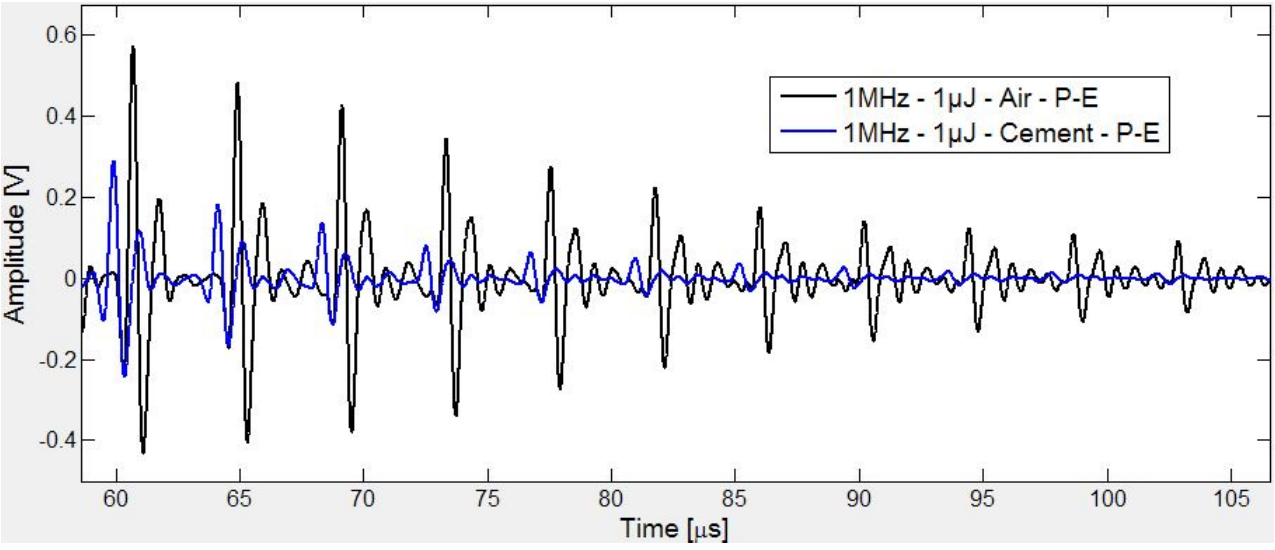

Figure 5.8: A closer look at the resonance ringing pulses showing the ringing with air and cement as annulus media

Figure 5.8 shows a closer look at the resonance ringing of the steel. The graph shows the ringing with air and cement as the annulus medium both at 1MHz and 1μJ energy. The series of pulses with cement in the annulus is considerably weaker that with air, this is as expected, because more energy is leaked into the cemented annulus with each reflection. Figure 5.9 shows the first reflection pulse from the steel with cement in the annulus. This is an example of how the 1MHz and 500kHz pulse gave different signal reflection. The frequency of the reflection is different; the length of the 1MHz pulse is about 2 μs while the 500kHz has a length of 4 μs. The frequency of the 1MHz is double of that of the 500kHz, which it should be. The strength of the signal is a lot weaker from the 500kHz than the 1MHz signal. The energy of the 500kHz pulse is 32μJ versus the 1MHz pulse of 1μJ, and the reflection pulse is still weaker than the 1MHz pulse. This might be caused by differences in the transducers; the diameter of the 500kHz element is for instance twice the size of the 1MHz. Same pulse trigger energy does not necessarily give the same transmitted energy in both transducers. The 500kHz transducer also tended to give less even sinusoidal waveforms which can be seen in figure 5.9.

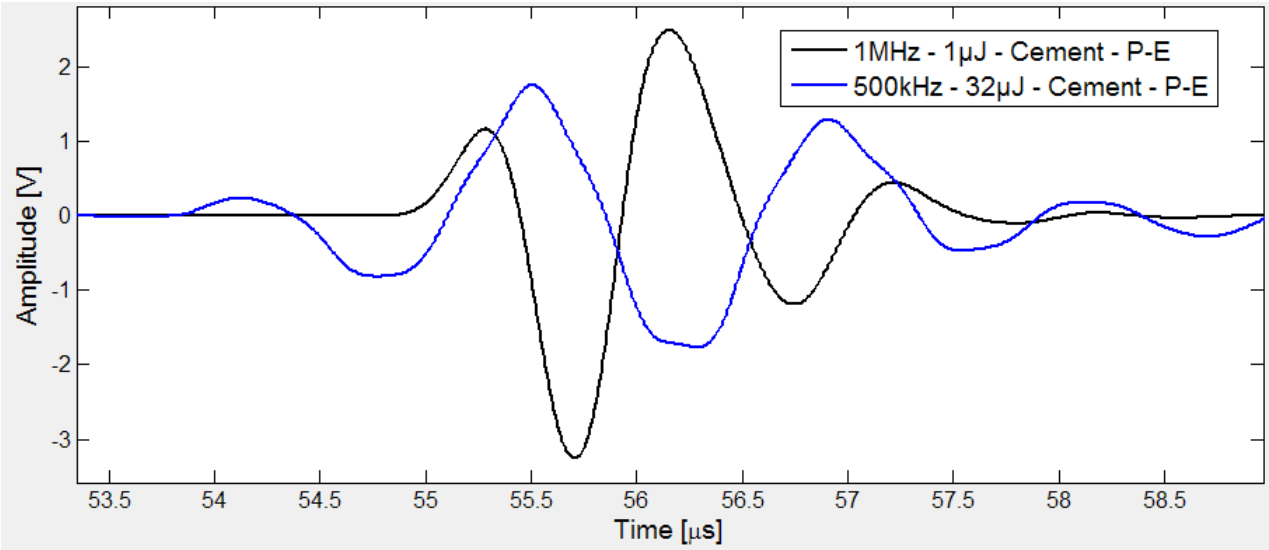

Figure 5.9: A closer look at the first reflection pulse with cement in the annulus at 1MHz and 500kHz

For this reason the results from the 1MHz and 500kHz measurements are presented individually. The data collected is interpreted and the following values are calculated:

5.2.1 Steel plate thickness

The following table 5.1 contains the data showing the two-way travel time of the compressional wave in the steel. This time difference can be used to calculate the plate thickness. The places where there is no value in the table are reflections that could not be distinguished from interference or the signal was too weak. Average time interval between each resonance pulse was 4.21

Time between reflections [μs]								
Reflection #	**1MHz air**	**500kHz air**	**1MHz water**	**500kHz water**	**1MHz mud**	**500kHz mud**	**1MHz cement**	**500kHz cement**
1	n/a	n/a	n/a	n/a	n/a	n/a	n/a	n/a
2	4.20	4.25	4.21	n/a	n/a	4.42	4.21	4.38
3	4.22	4.17	4.23	n/a	n/a	3.8	4.21	4.04
4	4.21	4.20	4.19	4.12	4.22	4.25	4.21	4.22
5	4.21	4.22	4.21	4.21	4.21	4.21	4.2	4.19
6	4.22	4.22	4.22	4.19	4.21	4.21	4.22	4.24
7	4.22	4.24	4.23	4.23	4.24	4.21	4.22	4.21
8	4.22	4.23	4.25	4.43	4.22	4.25	4.21	4.21
9	4.22	4.20	4.21	4.06	4.24	4.24	4.19	4.23
10	4.22	4.23	4.22	n/a	4.2	4.32	4.21	4.22
11	4.22	4.23	4.18	n/a	4.22	4.26	4.23	4.19
12	4.22	4.21	4.22	n/a	n/a	4.19	4.21	4.2
Average	4.22	4.22	4.22	4.21	4.22	4.21	4.21	4.21

Table 5.1: Table showing the time difference between each resonance pulse

μs for almost every set-up. The time interval represents the two-way travel time for the pressure wave inside the steel thickness. The steel plate thickness is therefore found by this simple calculation

$$h_{steel} = \frac{\Delta t}{2} \cdot v_{steel} \Rightarrow \frac{4.21\mu s}{2} \cdot 5.79 mm/\mu s = 12.18 mm$$

Velocity of a compression wave in steel is assumed to be 5790 m/s. The calculation gives a steel plate thickness of 12.18 mm. The measured steel plate thickness was 12.1 mm, measured with an electronic caliper. The measurement is accurate to less than 0.1 mm. The slight difference could mean that the steel thickness is maybe varying and perhaps slightly thicker in the center, or the steel speed of sound might be a tiny bit slower. There are of course a lot of possible causes for this slight difference.

5.2.2 Resonant frequency

Now that the two-way travel time is calculated, equation 3.5 is used to get the resonant frequency of the steel plate.

$$f_0 = \frac{1}{\Delta t} \Rightarrow \frac{1}{4.21\mu s} = 0.237MHz$$

The resonant frequency is found to be 237 kHz. The ideal transducer frequency would therefore be around 240 kHz for this casing, and would yield stronger ringing. Having a strong signal response is important when doing cement evaluation and it is therefore always used transducers with a frequency matching the casing thickness.

5.2.3 Signal attenuation

By measuring the peak to peak amplitude of each resonance pulse and plotting them against reflection number the following graphs are created:

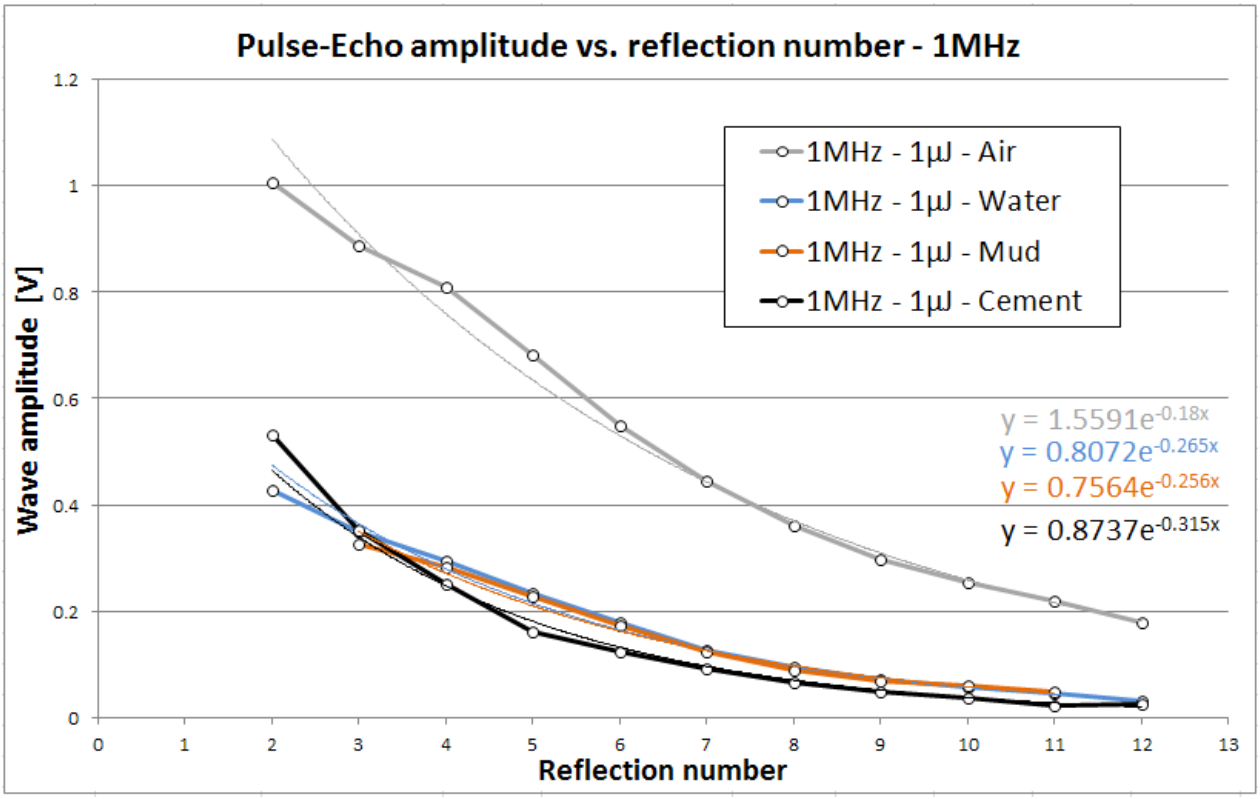

Figure 5.10: Amplitude of resonance ringing vs. reflection number of the different annulus media with 1MHz

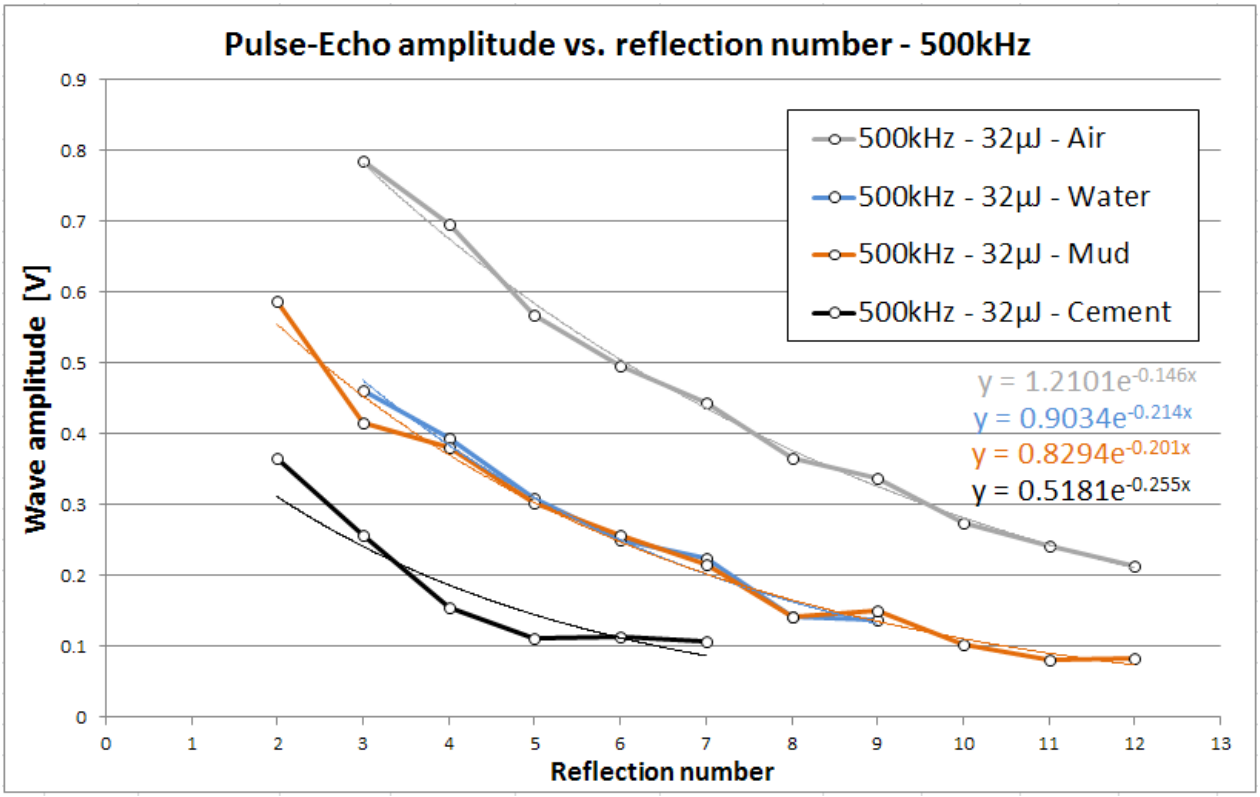

Figure 5.11: Amplitude of resonance ringing vs. reflection number of the different annulus media with 500kHz

The plotted lines in figure 5.10 and 5.11 are resembling exponential curves, and equations for the exponential curves the closest match the plots are found in the graph. These will later be used to find the attenuation of the signal. Another way to find the attenuation is to calculate the reflections coefficient between each resonance pulse and converting this to decibel attenuation. This should give a linear line when plotted against time or reflection number. The equation used to convert from reflection coefficient to decibel is:

$$\alpha = \log K_{ref} \cdot 20 \tag{5.1}$$

Where α is attenuation in decibel. Usually a multiplier of 10 is used, however, 20 is the multiplier used in the experiment since the power of sound is not measured directly in ultrasonic testing. The transducers produce a voltage that is approximately proportional to the sound pressure. The power carried by a travelling wave is proportional to the square of the pressure amplitude. Therefore, to estimate the signal amplitude change, the log of the reflection or transmission

coefficient is multiplied by 20. [13] This has been calculated in the following figures:

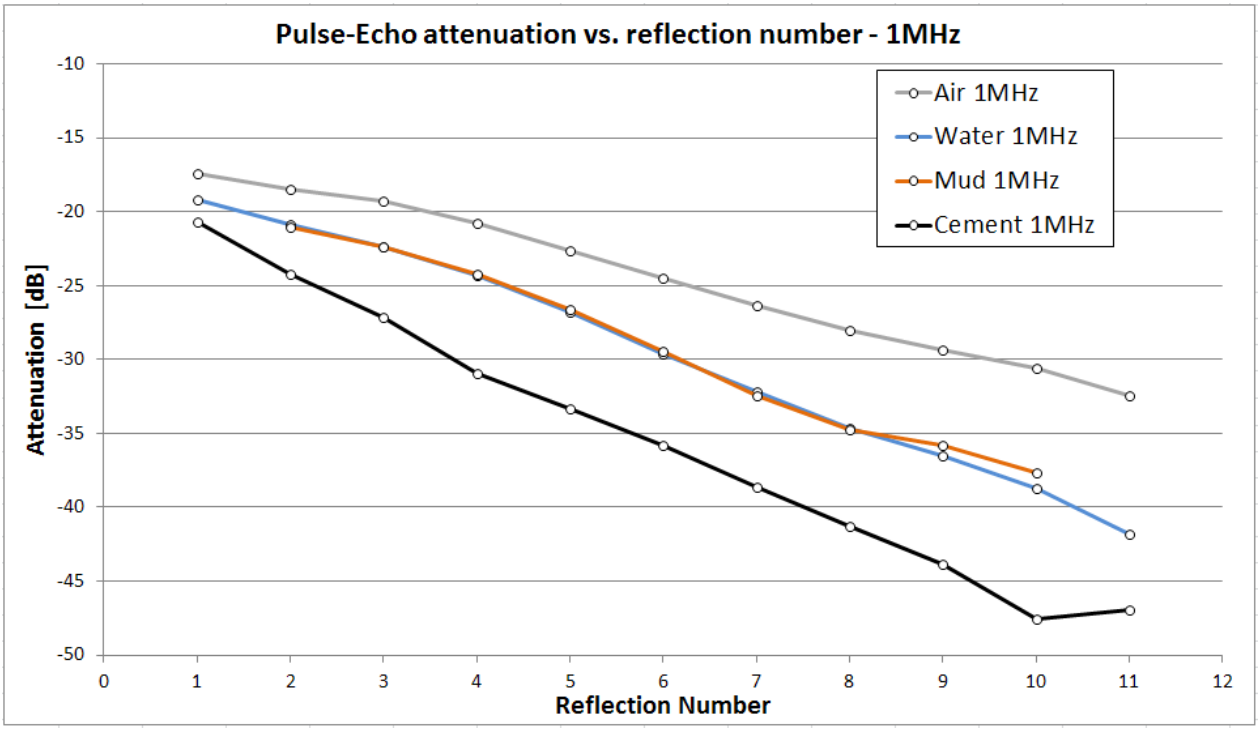

Figure 5.12: Attenuation of the pulses in decibel compared to the first reflection with 1MHz

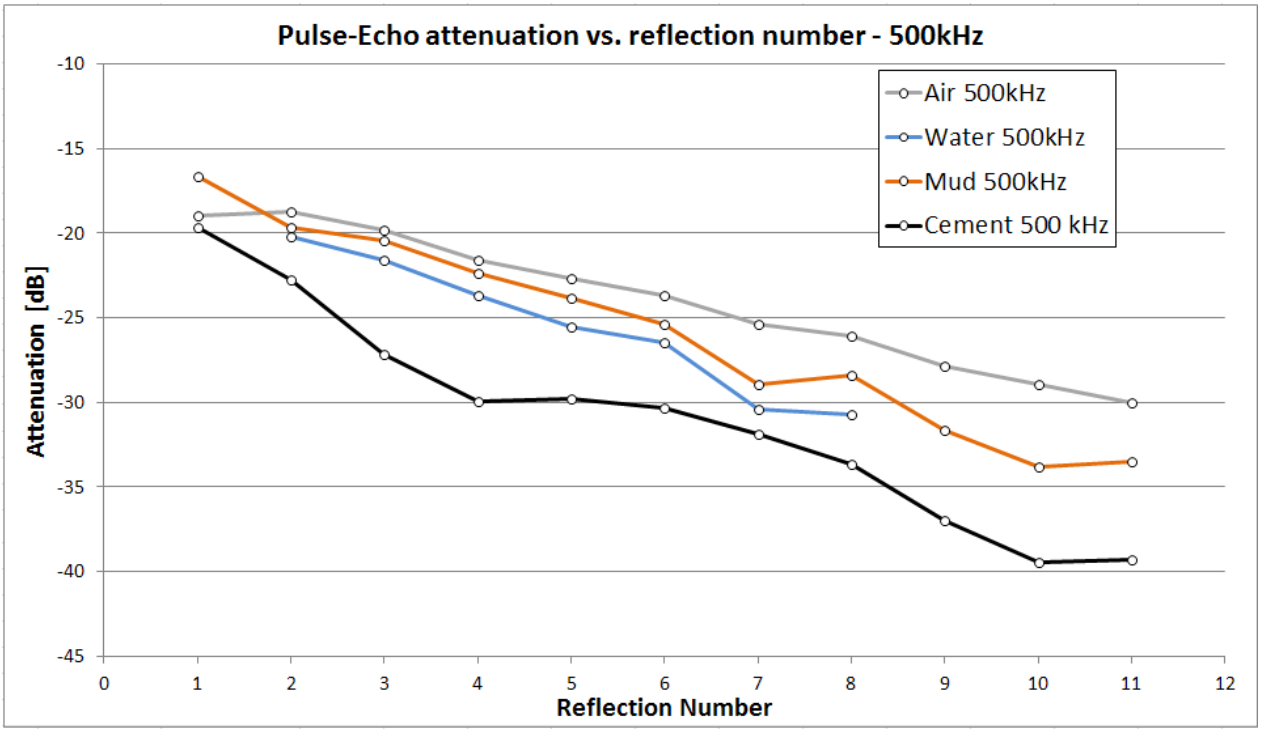

Figure 5.13: Attenuation of the pulses in decibel compared to the first reflection with 500kHz

The 1MHz measurements gave a more even exponential amplitude decay, giving linear attenuation plots in figure 5.12. Air in the annulus gave the least amount of attenuation, water and mud a bit more, and cement gave a the strongest signal attenuation. For the 10th reflection for example, air gave -31dB attenuation, water and mud around -38dB and cement -47.5dB attenuation from the first reflection. For the 1MHz measurements the water and mud set-up seem to give almost identical attenuation values. The 500kHz attenuation measurements for air, water and mud show a stable attenuation up to the 6th ringing. After that the attenuation varies more. This might be caused by the third interface reflection interfering with the signal. The same can be said of the cement attenuation which has the variation around reflection number 3/4.

Impedance is calculated by using equation 3.1, and the impedance for air, steel and water is theoretically 409 $\mathrm{N} \cdot \mathrm{s} \cdot m^{-3}$ (Rayl), 45.162 MRayl and 1.49 MRayl respectively. From measurements done on the mud and cement used (mentioned in section 4.3.1), the impedances are calculated to be 1.84 MRayl, and 5.41 MRayl respectively. The reflection coefficients between the different media is calculated with equation 3.2.

Interface	Steel-Air	Steel-Water	Steel-Mud	Steel-Cement
Reflection coefficient	0.999	0.876	0.849	0.618
Decibel reflection	-0.01	-1.15	-1.42	-4.18

Table 5.2: Reflection coefficients and corresponding decibel reflections between steel and other media

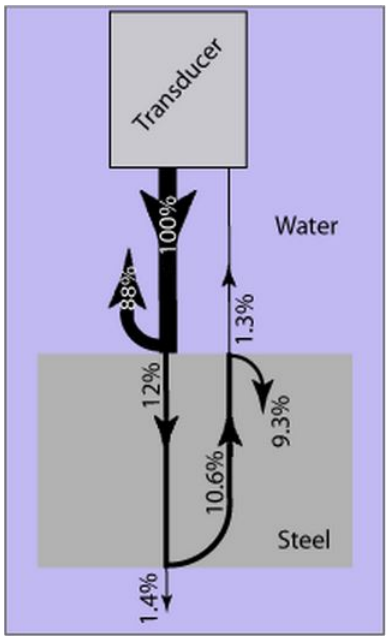

Figure 5.14: Illustration showing the transmitted and reflected percentage of initial wave energy though a steel casing wall surrounded by water[13]

From figure 5.14, illustrating the reflection and transmission of signal energy through a steel plate with water on each side, one can see that only $(1-0.876)\cdot 100 = 12.4\%$ of the initial compressional wave energy is transmitted into the steel plate. Had it been air on the other side it loses almost nothing (0.001 %) when it hits the steel-air interface, but loses another 12.4% when hitting the steel-water interface and this goes on and on until no energy remains inside the plate. When the steel plate has water on each side, it will now loose an extra 12.4% each time it hits the back of the plate. The same goes for mud and cement which the wave would lose 15.1% and 38.2% too, respectively. So by this logic, the peak-to-peak wave amplitude from the ringing signal with air, water, mud and cement behind should be 12.4%, 23.2%, 25.7% and 45.6% lower than the previous wave, respectively.

A good way to calculate attenuation is to find an exponential equation describing the amplitude vs. time plot. In figures 5.10 and 5.11 this has been done and the equation is

$$A = A_0 e^{-\alpha x} \tag{5.2}$$

A_0 is the initial unattenuated propagating wave amplitude and A is the attenuated amplitude after the wave has travelled a distance x from the initial location. α is the attenuation coefficient

of the wave travelling in the x direction. The dimensions of α are nepers/length and is converted to decibel/length by dividing by a factor of 0.1151. In this case it will be decibel per reflection.[13] Using this attenuation coefficient given by the equations in figure 5.10 and 5.11 the following graph was made to show the measured attenuation.

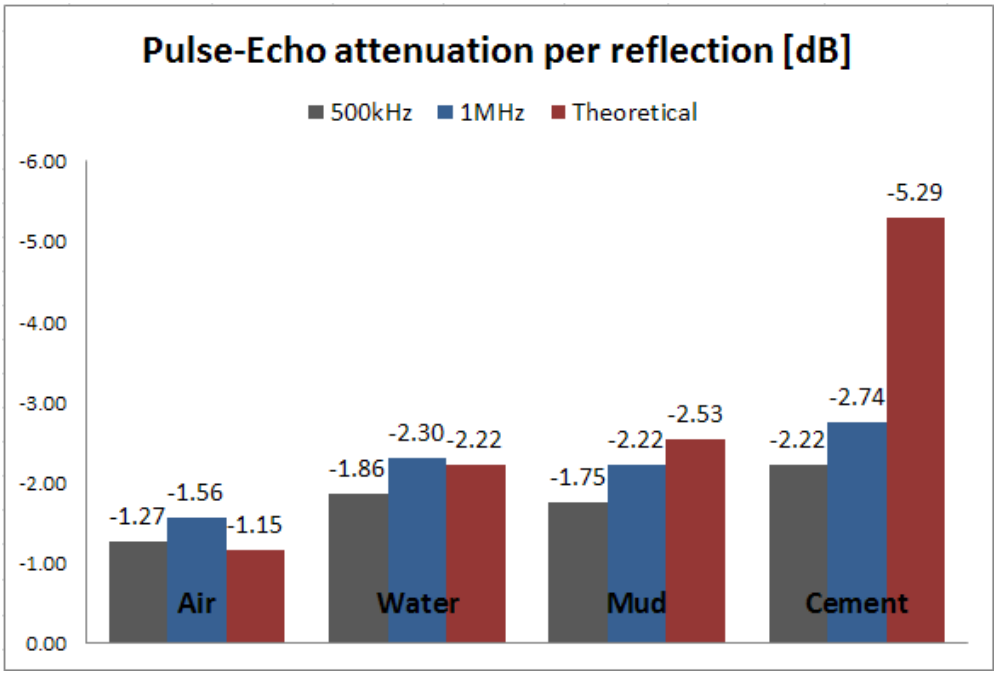

Figure 5.15: The average attenuation values measured on the BeCaLoS compared to theoretical values

From figure 5.15 one can see that the attenuation measured with air and water as the annulus media is a pretty good match with the theoretical attenuation. With mud and cement the results are a bit different from what one would expect the attenuation to be theoretically. It is strange that the mud measurements actually gave lower attenuation than water, and although the cement attenuation was clearly higher than the other measurements it is not nearly as high as one might expect. These results will be further discussed in chapter 6. Because the impedance of the steel casing is known, and the impedance of the logging fluid (water) is known, it is possible to calculated the impedance of the annulus material. This is done based on the measured attenuation and reflection coefficient between each pulse and solving for Z_2 in equation 3.2. It seems like the 1MHz frequency gave the best matching values. The impedance is a little high for air, but not bad, good enough to say that it is gas in the annulus. The water measurement gave $1.498 MRaly$ which is a very accurate impedance value for water. The mud impedance

Annulus material impedance [MRayl]	Air	Water	Mud	Cement
Calculated from P-E atteunation 1MHz	0.538	1.498	1.396	2.06
Calculated from P-E atteunation 500kHz	0.153	0.922	0.775	1.385
Calculated from density and velocity	0.0004	1.5	1.84	5.41

Table 5.3: Calculated material impedance values from the Pulse-Echo attenuation data

value is actually lower than water, this is odd and will be discussed more in chapter 6. At least the value is good enough to say that it is a fluid in the annulus. The cement impedance value of $2.06 MRaly$ is barely high enough to be able to say that it is a solid annulus, and not a liquid. But the value is much lower than the measured impedance of $5.41 MRayl$, which is a high density, fast cement. The values measured would suggest a low impedance, light weight cement, or perhaps very heavy mud. Microannulus might be the problem causer here, and this will be further discussed in chapter 6. The values measured with the 500kHz transducer give low impedances. It might seem that this transducer was not the best suited for this measurement, even though 500kHz is closer to the 240kHz resonance frequency of the plate and should theoretically yield stronger reflections. The reflections from the 500kHz were actually very weak, and 32μJ pulse energy had to be used to get good enough amplitude reflections. And even with 32μJ energy the pulses where low amplitude and after the 4th pulse the peak-peak signal was below 0.2V for most of the measurements. Signal going below 0.2V is starting to go into the noise regime of the oscilloscope, and values become less accurate.

5.2.4 TIE measurements

Because the annulus is fairly thin (less than 30mm) it should be possible to detect a TIE in the pulse-echo measurements. This will show as an interference in the resonance ringing, see figure 3.2. From analysing the amplitude measured in figure 5.11 it is possible to detect this interference. In the water and mud measurements, a decrease in amplitude is found in the 8th pulse reflection. This dip is not present in the air measurements, as is expected. Analysing the cement attenuation shows a dip in amplitude around the 5th pulse. Looking at the time of arrival difference between the dip and the first pulse it is possible to calculate the annulus thickness, when the annulus material compressional velocity is known. The annulus thickness was measured to

be 22.5mm during the water and mud measurements and 24mm during the cement measurements. The first pulse reflection arrives after 55.22μs and the 8th pulse arrives after 84.76μs. For the cement the values are 55.5μs and 72.33μs for the first and 5th pulse respectively.

$$h_{annulus} = \frac{\Delta t}{2} \cdot v_{water} \Rightarrow \frac{(84.76 - 55.22)\mu s}{2} \cdot 1.49 mm/\mu s = 22.00 mm$$

$$h_{annulus} = \frac{\Delta t}{2} \cdot v_{cement} \Rightarrow \frac{(72.33 - 55.50)\mu s}{2} \cdot 2.84 mm/\mu s = 23.89 mm$$

These time of arrival measurements give very accurate measurements of the annulus thickness, at least for water and cement. If borehole size is known this data can be used to find the compressional velocity of the material, and from the attenuation-calculated impedance; the density of the material can be found. The mud has a compressional velocity of $1418 m/s$ and would give a lower thickness measurement. It is not known why the 1MHz amplitude measurements (figure 5.10) did not show a TIE in the resonance ringing.

5.3 Pitch-Catch

The Pitch-Catch measurements were performed as explained in section 4.3.3 and 5.1. Several readings were done with varying transducer-receiver distance and with an incident angle of 30 degrees. The TIE results will be presented at the end of this section. The steel plate wave measured gave a compact pulse with changing phase velocity. The TIE was only observed at higher transducer-receiver distance, which will be explained later.

5.3.1 Waveform analysis

The waveform of the pulse was stable and with decreasing amplitude as the wave propagates along the steel plate.

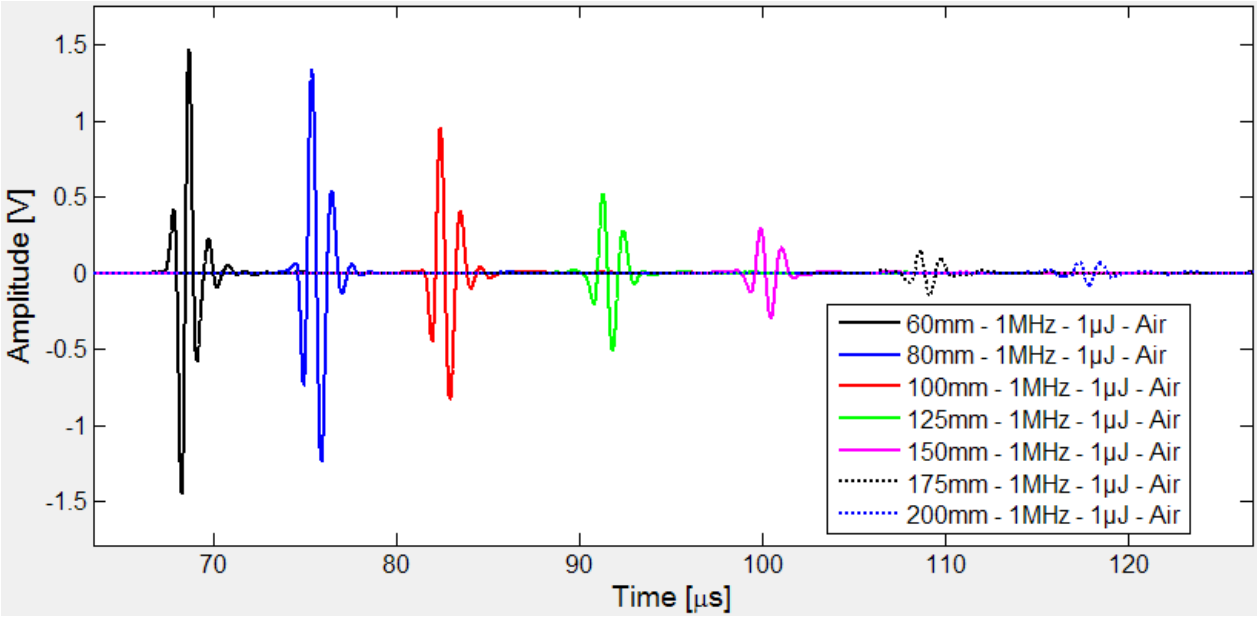

Figure 5.16: 1MHz pitch-catch signals at varying t-r distance with air as annulus media

Figure 5.16 shows the compactness of the flexural wave signals and how the waveform stays the same with varying distance. The readings with air in the annulus has been chosen to show this because they gave the highest signal amplitude.

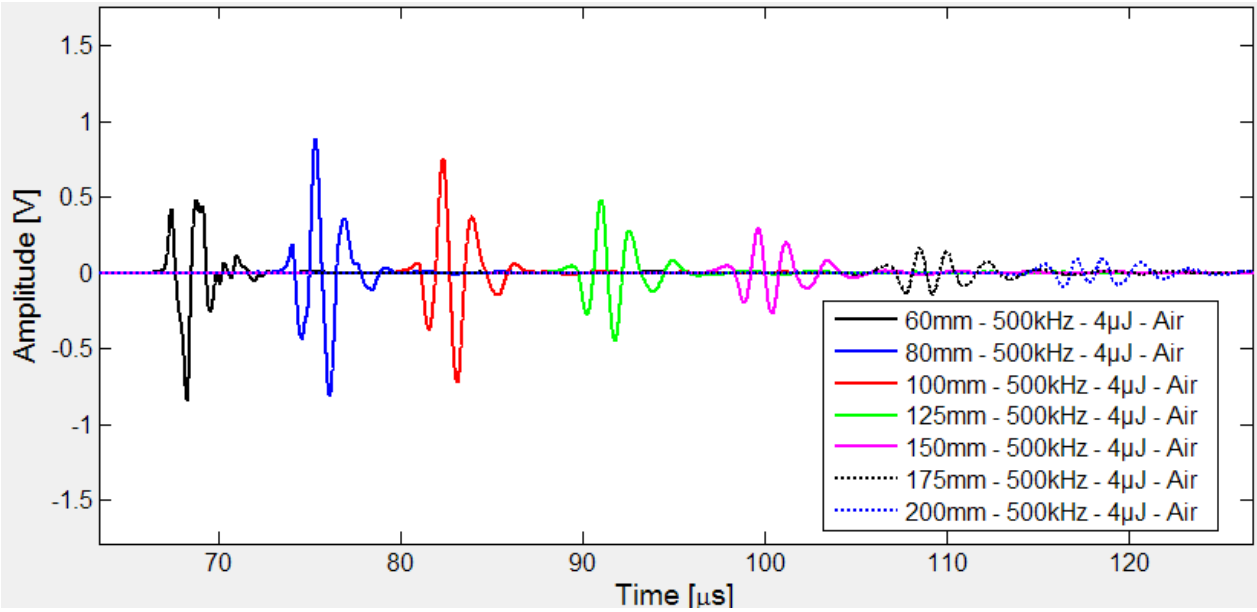

Figure 5.17: 500kHz pitch-catch signals at varying t-r distance with air as annulus media

With 500kHz in figure 5.17 the first pulses show a lower amplitude. The measurement done at 60 and 70mm distance do not have a clear compact waveform, but this levels out at 80mm which

has the strongest amplitude. The waveforms recorded for both 500kHz and 1MHz where the same as figure 5.16 and 5.17 for all annulus materials, only the amplitude was different. Taking a closer look at the first plate wave signal:

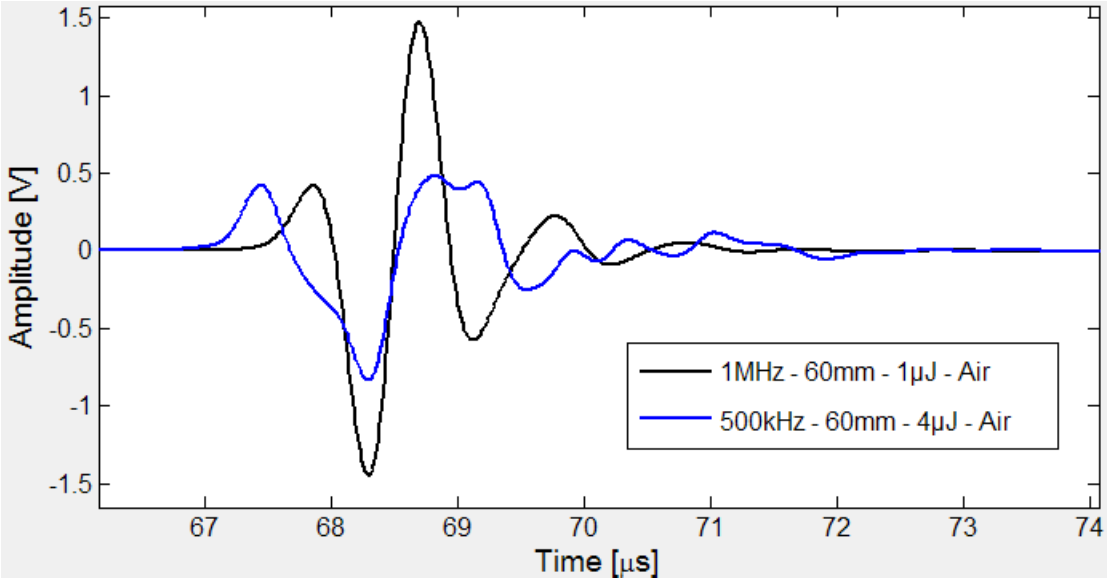

Figure 5.18: Waveform of the two plate wave signals at 500kHz and 1MHz at 60mm

From this figure 5.18 it is evident that the 500kHz pulse seems to suffer some interference. Analysing the two signal's frequency spectrum give more information.

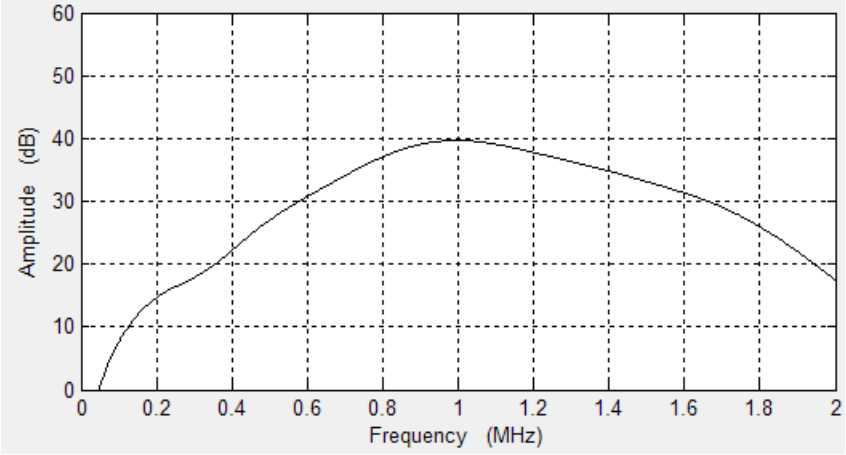

Figure 5.19: Frequency spectrum of 1MHz pulse at 60mm

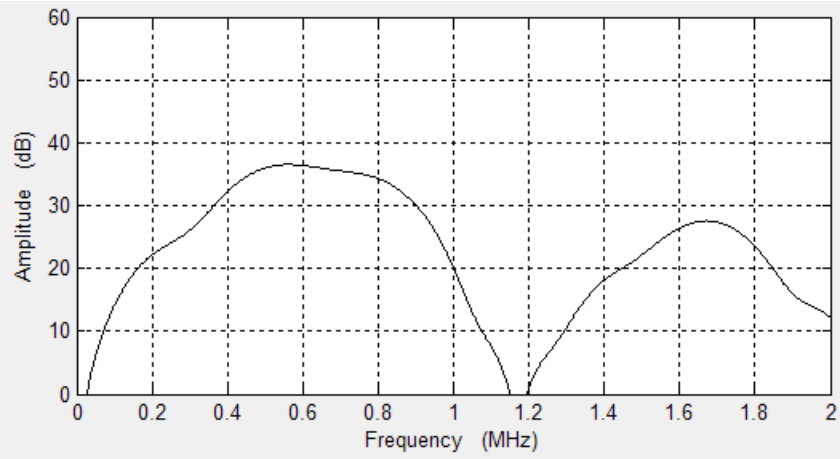

Figure 5.20: Frequency spectrum of 500kHz pulse at 60mm

Figure 5.19 show that the 1MHz pulse is a broadband pulse, strongest around the central frequency of the transducer at 1MHz. The 500kHz transducer frequency spectrum in figure 5.20 show a strong frequency amplitude around 500kHz, but also a strong frequency component around 1.7 MHz. The 500kHz component is around 37dB in amplitude, while the 1.7MHz is 28dB. This is significant enough to cause the waveform to take the shape seen in 5.18. The plate wave is dispersive, and this should cause the 1.7MHz component of the pulse to weaken. Next is a look at the signals at 125mm transducer-receiver distance.

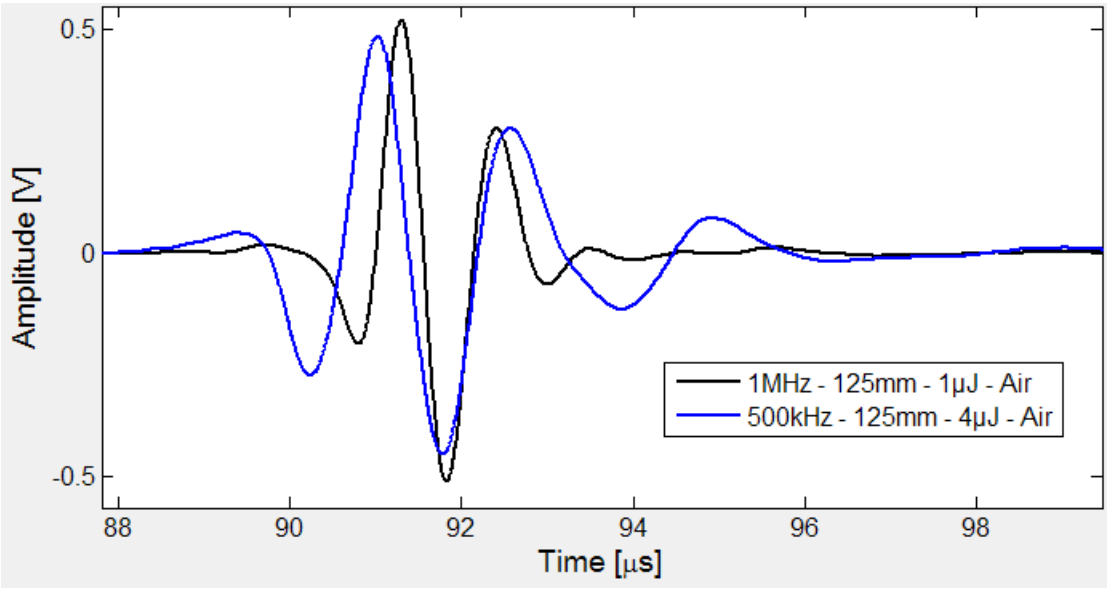

Figure 5.21: Waveform of the two plate wave signals at 500kHz and 1MHz at 125mm

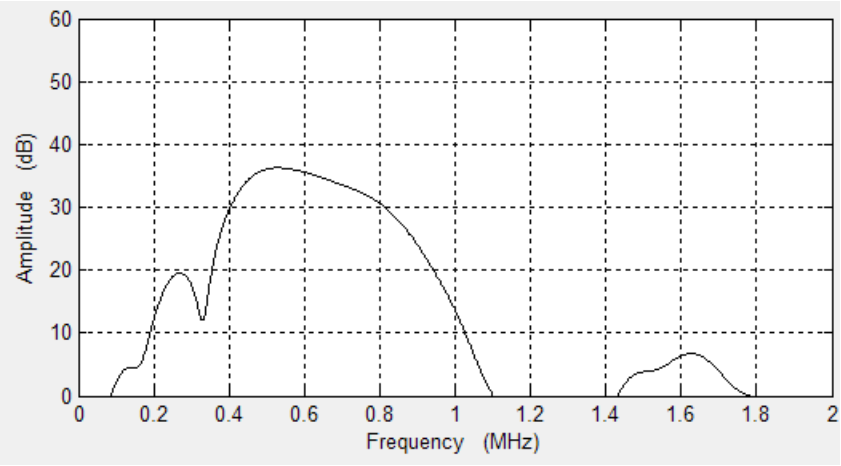

Figure 5.22: Frequency spectrum of 500kHz pulse at 125mm

From these two figures 5.21 and 5.22 it can be seen that the high frequency component of the 500kHz pulse is lost. The signal appears much more compact and sinusoidal. The 500kHz component in the frequency spectrum is still at around 37dB, but the 1.7MHz component is down to around 8dB. This effect and what impact is had on the results will be discussed in chapter 6.

5.3.2 Attenuation

The amplitude vs. transducer-receiver spacing results were as follows:

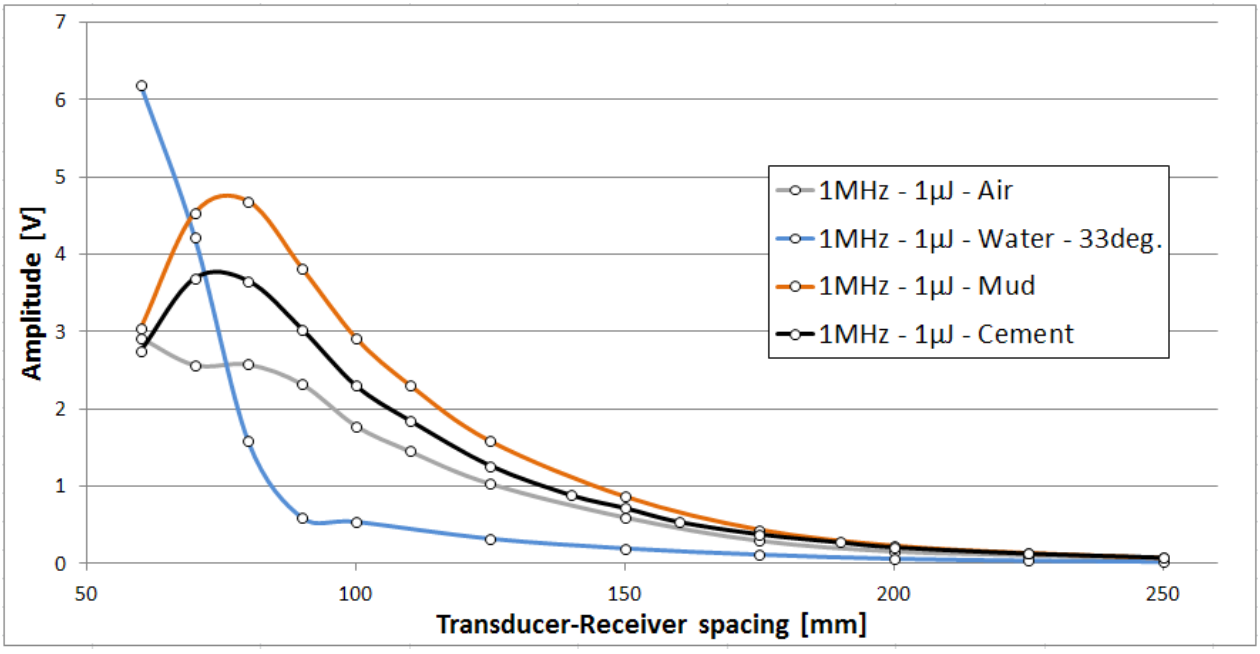

Figure 5.23: Plate wave amplitude vs. t-r spacing with 1MHz pulse

From the 1MHz amplitude vs. transducer-receiver spacing data it is evident that the attenuation for each annulus media looks to be quite similar. The measurements with water in the annulus with the 1MHz transducers were performed with 33 deg incident angle. This was done before it was discovered that 30 deg was the optimal angle. The water plot is different from the others because the amplitude drops quickly to low values. The other measurements show that the pulse increases in amplitude the first 30mm before exponentially decreasing to a low amplitude. This could probably be caused by the flexural wave needing to propagate and resonate through the plate thickness a few times before reaching its full amplitude. The flexural mode in not induced immediately upon first impact with the incident pulse.

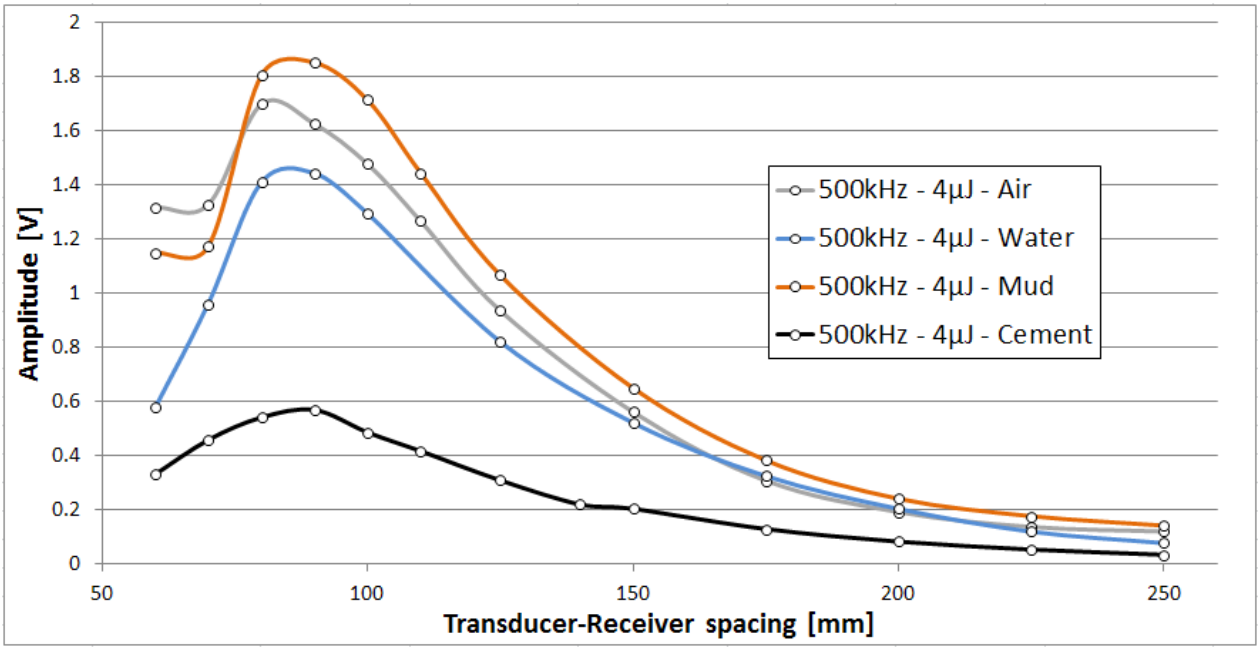

Figure 5.24: Plate wave amplitude vs. t-r spacing with 500kHz pulse

The 500kHz measurements show the same amplitude peak after propagating 30-40mm as the 1MHz measurements do. This is probably caused by a combination of the above mentioned need to propagate to reach full flexural mode, and the pulse frequency scattering effect mentioned in subsection 5.3.1. The attenuation rate seems to be fairly even between the four plots. The plate wave amplitude is higher for air-fill annulus than for water-filled. The water-filled plate wave amplitude is also higher than the cement-filled amplitude. The steel plates flexural ease of motion is lower when cement or water is present in the annulus, and that would give a lower amplitude. Why the measurement with mud in the annulus gave the highest amplitude

flexural wave is not known, but there are a lot of variables to this experiment, and it will be discussed further in chapter 6. To find the attenuation of the plate wave in decibel per length the same method as in subsection 5.2.3 is used. Exponential equations that best matches the plotted lines in figure 5.23 and 5.24 (starting from the highest amplitude) are found. Using equation 5.2 and the attenuation coefficient the following values are found:

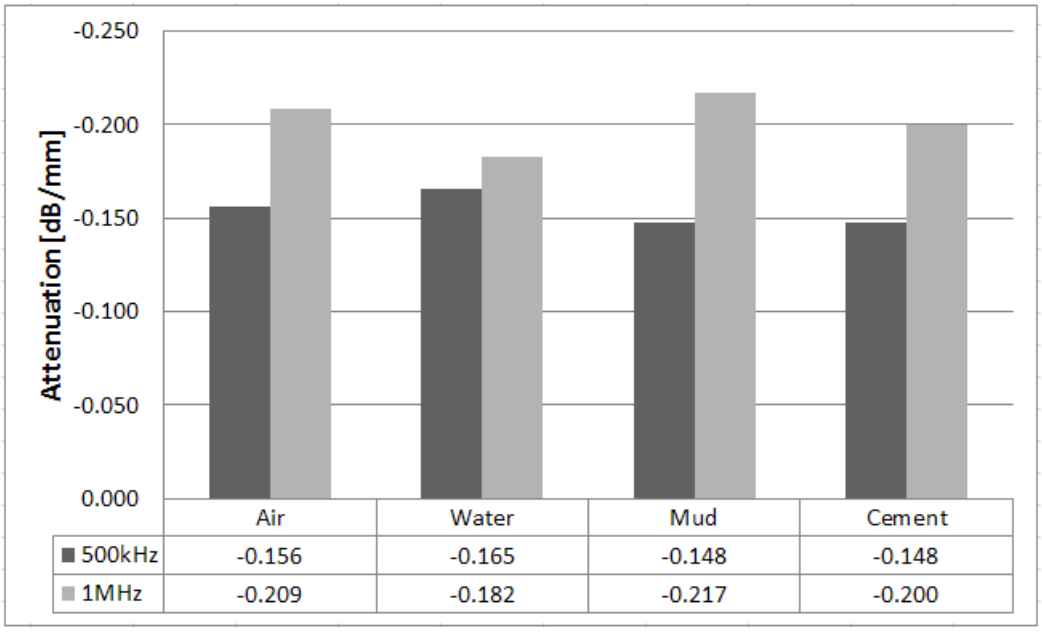

	Air	Water	Mud	Cement
500kHz	-0.156	-0.165	-0.148	-0.148
1MHz	-0.209	-0.182	-0.217	-0.200

Figure 5.25: Pitch-Catch flexural wave attenuation values in dB/mm

Figure 5.25 show how even the attenuation values of the different measurements were. It is not easy to say anything about the content of the BeCaLoS by looking at the plate wave attenuation alone. The values are also strange. Air as an annulus media should theoretically give low attenuation, but here it shows a higher attenuation than cement. The attenuation value for mud and cement at 500kHz is actually identical, but checking with the flexural wave amplitude in figure 5.24 it is obvious that there must be two completely different annulus materials present. The attenuation values are higher for the 1MHz measurements than the 500kHz as is expected by a higher frequency. A higher frequency pulse will lose more energy as it propagates. The impedance of the cement cast in the BeCaLoS was measured to 5.4MRayl, with a compressional wave velocity of 2840m/s. This would be past the "evanescence point" explained in section 3.3.4 and illustrated in figure 3.8. This would mean that only shear waves are transmitted into the cement annulus and the attenuation is dropped to small values. At 5.4MRayl figure 3.8 predicts

attenuation values even lower than water. This is true for the 500kHz measurements found in this experiment, and can explain why the cement attenuation values are so low. The cement amplitude is the lowest, as expected from a solid material annulus, but the attenuation shows a fluid. This data would have to be compared to the pulse-echo data to determine the annulus material. And the pulse-echo values indeed show values comparable to a solid.

All in all, it looks like the 12mm thickness of the steel plate might be too thick to give good sensitivity to the annulus material. The values of the attenuation are very similar, regardless of annulus material. But evanescence point and low difference in impedance of water and mud might also be a factor here. Further discussion in chapter 6.

5.3.3 Phase velocity

The average phase velocity of the plate wave was also calculated from all the measurements. This was done by calculating the distance the wave propagates in the steel at each transducer-receiver interval. The travel time will be 2 times the distance from the transducer element to the steel plate divided by the speed of sound in water, plus steel plate propagation distance divided by the phase velocity of the flexural wave. All of these values are know except phase velocity and it is solves for. This gave the following values:

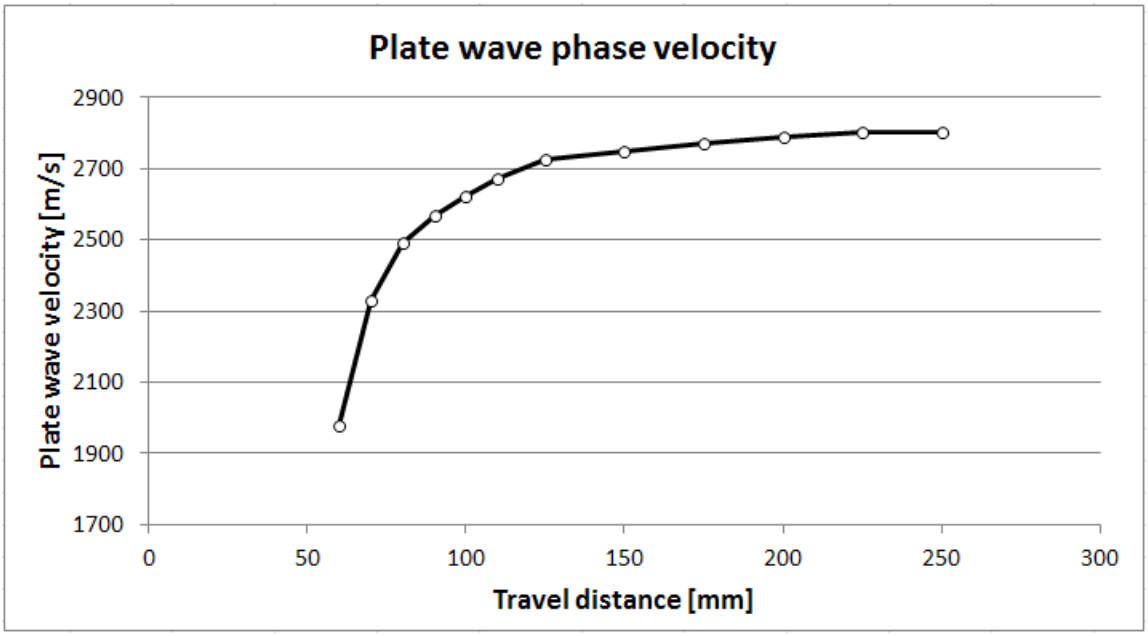

Figure 5.26: Plate wave phase velocity vs. propagation distance

The plate wave phase velocity increases as it propagates along the steel plate. The first 30mm it accelerates from 1980 m/s to 2500m/s and seems to reach a maximum around 2800 m/s. This increase in velocity also corresponds to the increase in amplitude shown in figure 5.23 and 5.24. This phenomenon of phase velocity increase further strengthens the theory that the flexural wave needs to propagate a certain distance before it reaches its correct mode and leaks as much energy as it can. From the Reissner-Mindlin thick plate models mentioned in section 3.3.2 the theoretical phase velocity of the flexural mode was found to be 2750 m/s. The lab experiment confirms this velocity.

5.3.4 Third Interface Echo

In this section the TIE results will be presented. TIE pulses were observed in the measurements with water, mud and cement. Air in the annulus obviously did not show any echo. The echoes were weak in amplitude and sometimes only detectable at the highest pulse energy of 32μJ. For this reason, all the data collected from the TIE measurements were done at 32μJ energy. The following figures show some TIE waveforms:

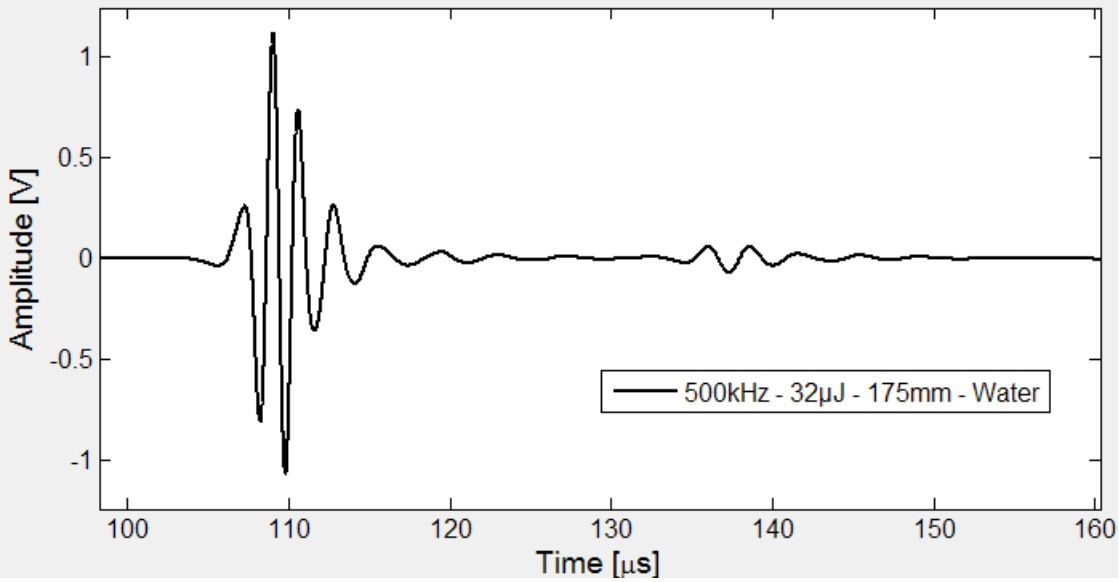

Figure 5.27: Waveform showing a TIE at 500kHz with water-filled annulus

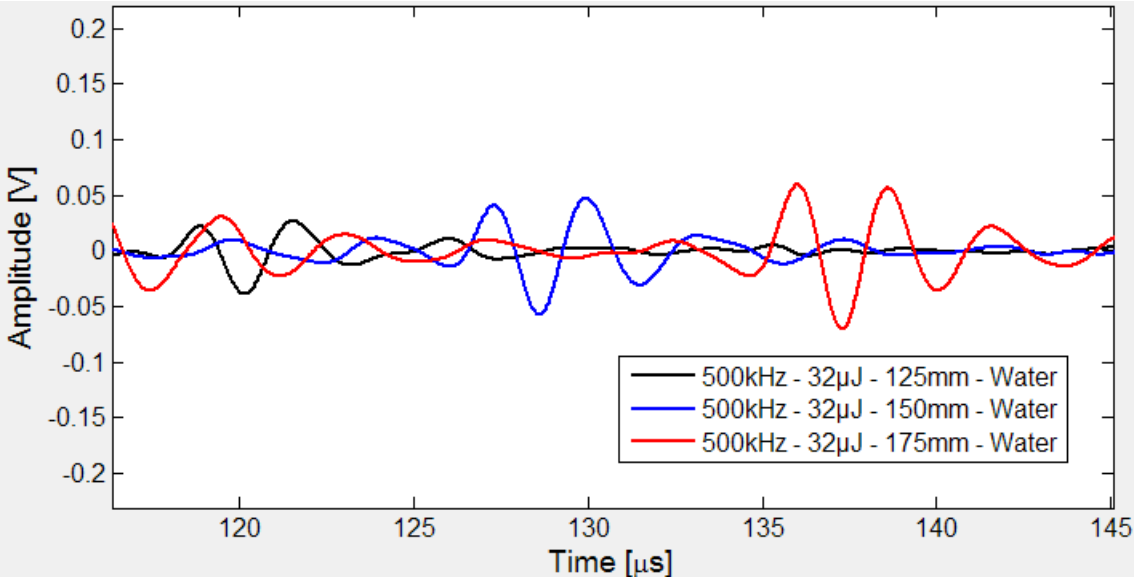

Figure 5.28: Close-up of the TIE waveforms with different t-r spacing at 500kHz

The amplitude values of all detectable TIEs are recorded giving the following plot:

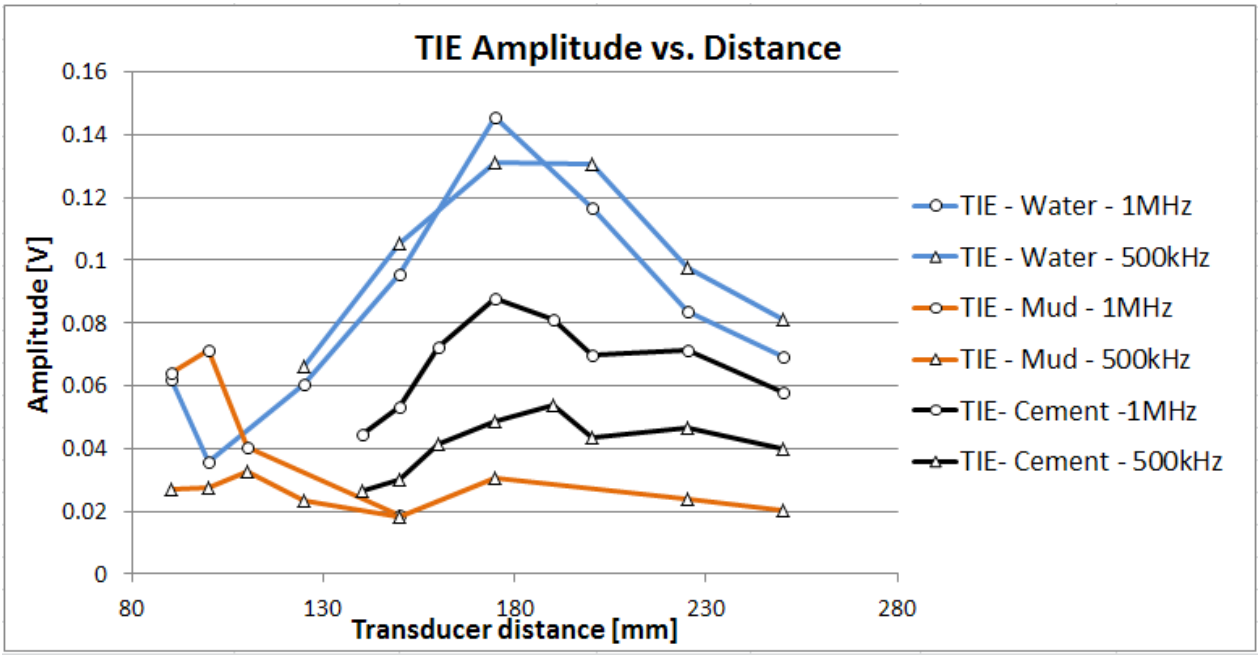

Figure 5.29: TIE amplitude vs. t-r distance for all BeCaLoS set-ups

Figure 5.29 shows a peak in amplitude around 175mm transducer distance. This is around 30-40mm after the first signal is detected and might be caused by the same reason the plate wave amplitudes have a peak after 30-40mm distance. The water annulus TIE is the strongest,

followed by the cement and then the mud. This is logical because water has the least attenuation, and mud has the largest. The mud TIE is very weak, and at some distances the TIE could not be distinguished from signal noise. The delay of the TIE compared to the plate wave represents the time it took the compressional wave (or shear wave) to travel from the plate to the formation and back. The next plot shows the recorded delay values from the measurements:

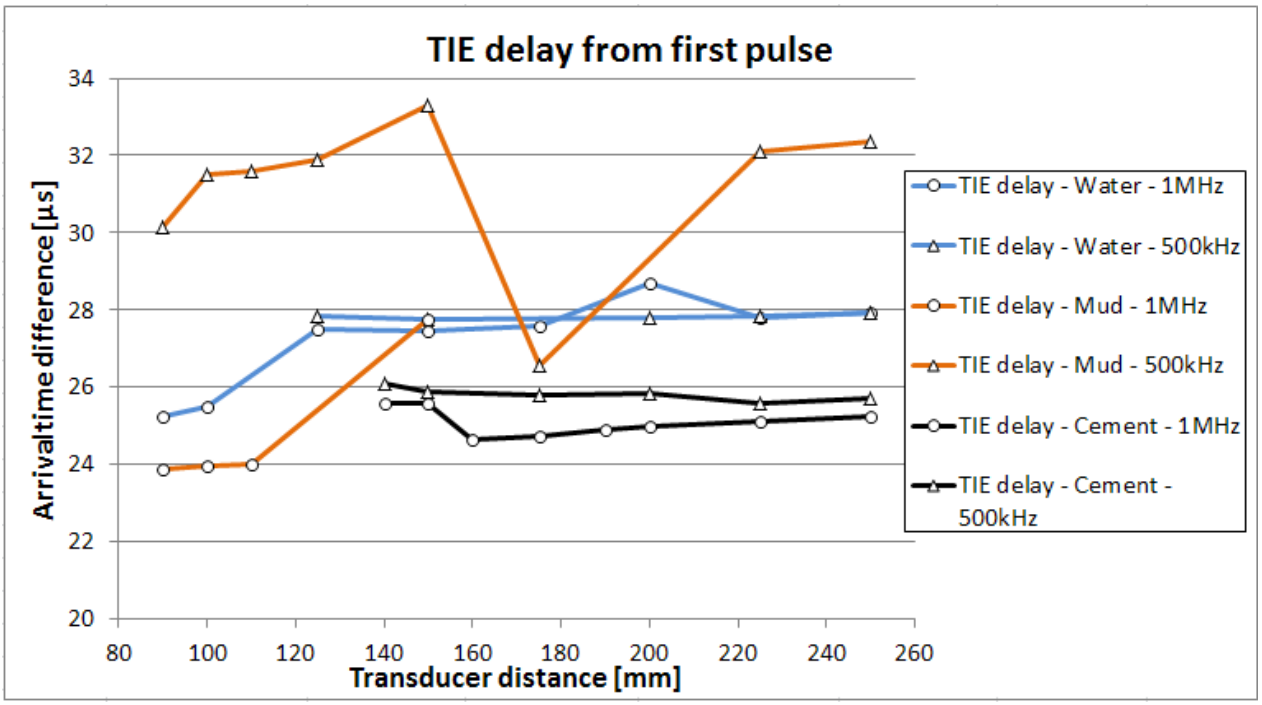

Figure 5.30: TIE time delay from the first plate wave vs. t-r distance

The delay is fairly constant with changing transducer-receiver distance for water- and cement-filled annulus but a bit more changing for the mud measurements. It should be noted that the mud measurements were very low amplitude and difficult to distinguish. This value of TIE delay can be used to calculate the annulus thickness when the annulus material speed of sound is known. Likewise if the borehole diameter is know, the annuls material speed of sound can be found. Calculating the cement annulus thickness as an example: For the 500kHz measurement the average TIE delay was 25.8μs and it is expected that only the shear wave propagates through the annulus because of the high impedance cement. The shear wave velocity in class G neat cement is around 2.0 mm/μs.[1] The distance the wave has travelled is therefore $25.8\mu \cdot 2.0mm/\mu s = 51.63mm$. This value is divided by two to find the one-way distance. The wave does not travel straight down, and using Snell's Law the incident angel of the shear wave in

the cement is found to be 41.8 deg. Now the annulus thickness is found by multiplying the one-way travel distance with the cosine of the incident angle. $\frac{51.63mm}{2} \cdot \cos 41.8 = 19.2mm$. This method is used on all the average TIE delay values and are presented in this table: The annulus

Average TIE delay	Water [µs]	Mud [µs]	Cement [µs]
500 kHz	27.8	31.2	25.8
1 MHz	27.2	24.9	25.1
Calculated annulus thickness	**Water [mm]**	**Mud [mm]**	**Cement [mm]**
500 kHz	18.1	19.5	19.2
1 MHz	17.7	15.6	18.7

Table 5.4: TIE delay and corresponding annulus thickness calculation for the different measurements

thickness values calculated from the 1MHz TIE data are lower than the 500kHz values. It seems as though the 500kHz frequency give better TIE values, because values around 19-20mm are not bad compared to the measured annulus thickness of 22.5-24mm.

6 | Discussion

The experiments conducted are simple enough in execution, but very complex and full of variables when trying to analyse wave-path and amplitude change. Where did the wave actually propagate? At what interfaces did it lose energy, and how much? These are questions that are very difficult to answer from physical lab experiments. Both the pulse-echo and pitch-catch method was performed successfully, and the results spur more questions and call upon more experiments to be conducted. There are a lot of possible causes for error in the measurements done here and the results of the experiment will be further discussed in this chapter.

In section 4.3.3 the theoretical best incident angle for exciting a flexural wave was found to be 33 deg. Why is it that the experiment found that angle to be 30 deg.? This is not obvious, but it might be caused by a mixing of modes. While it is practical to think that the only mode excited is the flexural, but a lot of mode are present at the frequencies used in this experiment. This is shown in figure (XX), and these modes travel at a much higher velocity. At the moment of impact with the thick steel plate, the right phase velocity to use is equation 3.18 might actually be higher. For very low frequencies (very thin plates) the phase and group velocities are both proportional to the square root of the frequency; the group velocity is twice the phase velocity. This simple relationship is a consequence of the stiffness/thickness relationship for thin plates in bending. At higher frequencies where the wavelength is no longer much greater than the plate thickness, these relationships break down. The phase velocity rises less and less quickly and converges towards the Rayleigh wave velocity in the high frequency limit.[19] 500kHz and 1MHz have reached the limit at the Rayleigh wave velocity, which is approximately 92% of the shear wave velocity. Using this value in equation 3.18 gives:

$$\sin\theta = \frac{v_f}{c_{S_steel} \cdot 0.92} \Rightarrow \theta = \arcsin\frac{1490 m/s}{3260 m/s \cdot 0.92} = 29.7\,\text{deg}$$

This might show that the Reissner-Mindlin value of 2750m/s is wrong to use, and the Rayleigh wave velocity is the correct phase velocity. However, the phase velocity was measured to be 2800m/s, although it did start at a low velocity.

The mud measurement gave strange results and proved to be a difficult annulus media to deal with. The impedance was measured lower than water from the P-E measurements, but with attenuation very similar to water in figure 5.12 with 1MHz. The mud used had a very high attenuation. This was actually measured (with difficulty) in the lab to be almost 10dB/cm, but the equipment used was not meant for fluids so the value might be inaccurate. One obvious weakness of the BeCaLoS is that it is horizontal and not vertical. It is possible that during the measurements the mud settled inside the tank and had almost water-like properties at the steel-mud contact. The high attenuation of the mud was problematic for the TIE measurements, where it gave very low amplitude signals, and in figure 5.29 the 1MHz signal could not read anything past 150mm.

While the P-E measurements did show a higher attenuation for the cemented annulus experiment, it did not show as high as expected. This is probably caused by the presence of a microannulus. The cement used stated that it would shrink about 1% during hydration. 1% is significant, and probably enough to create a small microannulus. The BeCaLoS was left to set tilted, in the hope of that the cement would only shrink in the top, leaving a good bond along most of the steel plate. This probably did help, because the flexural wave amplitude is a lot lower for the cement measurements. The best way to prevent the cement shrinkage creating a microannulus would probably be to cast the cement while the BeCaLoS is upside-down. Also, to inject water into the annulus after the cement has set to create a better acoustic bond in areas where there might be a small microannulus. This experiment was performed without water present, and might have increased the effect of the microannulus.

Another strange find from the experiment data is from the pitch-catch data. The attenuation is very similar regardless of annulus content, but the plate wave amplitude is very different. From the 500kHz measurements especially (figure 5.24), the annulus material seem to effect the amplitude. Theoretically the plate wave amplitude should start around the same value, but have different attenuation as it propagates. In the experiment it was found that the initial amplitude is different and the attenuation is almost the same. The author has not found any sources

mentioning the initial flexural amplitude as a way of determining annulus material, only attenuation. The stiffness of the plate must be affected by the annulus media and this would surely have an impact on the flexural amplitude. This might be something to look into.

The reason the flexural attenuation values measured are so similar probably has to do with the low sensitivity of such a thick plate as 12mm. It fails to distinguish between mud, water and air and it would probably be better to have a thinner steel plate. From the COMSOL simulations in figure 5.3a the bending motion of the plate seems to be a lot stronger at the top of the plate than on the bottom. The motion of the plate wave might not be fully flexural, and this can cause the wave to be less attenuated from the annulus than is expected. The combination of a thick plate and this weak bending effect could be the cause of the low sensitivity to the annulus materials.

The low cement attenuation is probably due to the cement impedance being above the critical impedance as mentioned before. This should cause values even below water attenuation, which it does.

Lastly, the effect of increasing amplitude of the initial plate wave, and TIE observed on all pitch-catch measurements is discussed. The effect is most likely caused by a combination of resonance of the flexural wave and the initial excitation of several higher-order modes. The flexural wave need to propagate a small distance in the steel plate before it reaches its highest amplitude, the same way the 2 first P-E reflections are weaker than the third. Also, the higher-order modes probably interfere with the flexural mode and after a short propagation in the steel these are lost to dispersion; leaving the flexural wave free to propagate at full amplitude. Tonni F. Johansen did a simulation in COMSOL which shows this effect. The following images are snapshots from a simulation animation, simulating a 500kHZ pulse hitting a 12mm steel plate surrounded by water at 30 deg. incident angle. Figure 6.1 shows the delay with weak amplitude right after the initial steel reflection, before the strong signal shows later illustrated with "plate wave". This confirms that plate wave does not immediately reach full energy dispersion, but after a short propagation. From the figure it is also evident that the signal reflected into the annulus is weaker than the signal reflected on the top. The colour scale difference show stronger pressure on the top "Plate wave" than the illustrated "weaker signal". The simulations further showed that the same happens to the TIE.

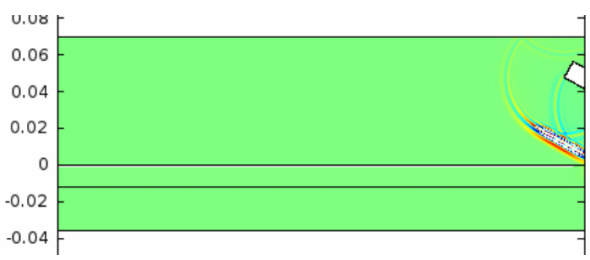

(a) Initial pulse about to hit the steel plate

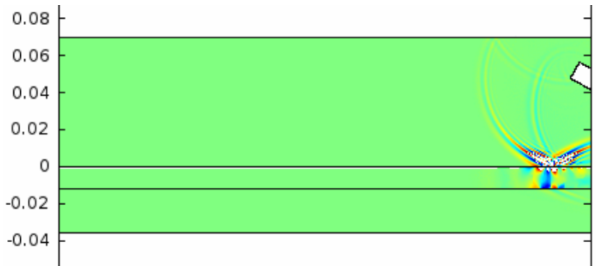

(b) Pulse has hit the plate

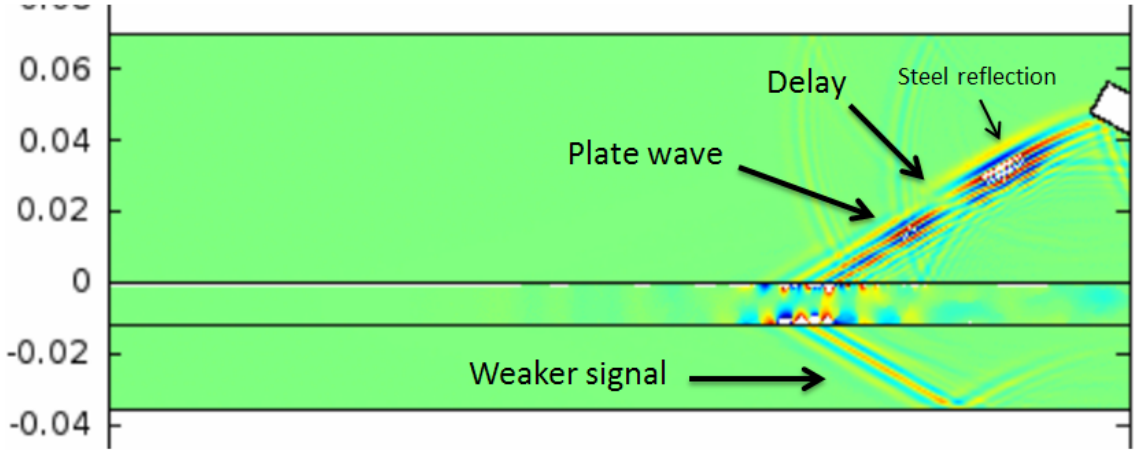

(c) Snapshot of simulation with added figures

Figure 6.1: Snapshots from COMSOL simulation animation showing incident pulse and resulting reflections

7 | Summary, Conclusion and Future Work

The field of well cement evaluation is struggling to keep up with the fast advancement in cementing technology. Few tools are being developed, and oil companies are questioning the reliability of the measurement results. Ultrasonic tools using pulse-echo and flexural wave attenuation is used to predict the impedance of the cement behind the steel casing. High impedance is related to good quality cement. The pulse-echo technique gives information on tool eccentering, casing conditions and cement bond present. Flexural Lamb waves are waves that propagate by flexing the entire casing. This causes good contact between casing and the surrounding media, and is very dispersive. This good contact, and the nature of the flexural wave causes the wave to be less affected by microannulus and being able to detect lower impedance mud. The third interface echo can provide information about the annulus material and borehole thickness. Because it reflects from the annulus-formation interface it is also able to detect washouts. This reflection is however very sensitive to tool eccentering and high attenuation annulus materials.

The lab experiments proved the ultrasonic leaky Lamb flexural wave and pulse-echo theory correct, and the different methods were performed successfully. The results highlighted some obvious weaknesses of the ultrasonic evaluation; including large casing thickness, highly attenuating annulus material, microannulus and Lamb-mode uncertainties. The pulse-echo experiment gave adequate results on annulus material and was able to distinguish between gas, fluid and solid annulus. Third interface echo data also gave accurate borehole thickness values. The cement measurements indicated the presence of a microannulus.

The pitch-catch experiment showed some problems with exciting the correct flexural mode with the frequencies of 500kHz and 1MHz. Large casing thickness gave low sensitivity on wave attenuation and annulus material characterization was difficult. The cement measurements

did show low attenuation values caused by high impedance cement; illustrating the importance of using both pulse-echo and pitch-catch to determine well integrity conditions. Third interface echoes were recorded successfully and gave a pretty accurate annulus thickness value. A question was raised to whether the amplitude of the initial flexural wave can be used to give information on annulus condition.

Even though this experiment was performed on media with defined properties and under ideal conditions, the results were still difficult to interpret. When performed in mud with uncertain properties, casing with uneven surface and on foamed cement with microannulus, one can imagine the difficulty of getting good evaluation results. With the coming increase in need for P&A operations, this would certainly be a good time for oil companies and service companies to start investing in research related to cement evaluation. There is great development potential in ultrasonic measurements, and the flexural wave technique might just be the start of something big.

Future Work

There is a lot of work that can be done with the BeCaLoS further investigate these measuring methods. Doing the same experiments with a thinner plate would be preferable, to see if the attenuation values are then more distinguishable. To really test how well the flexural wave radiates energy into the annulus it would be interesting to do a measurement with the receiving transducer on the other side of the steel plate. If a relationship between top and bottom wave energy radiation is found, the TIE amplitude measurements can give information on formation impedance. In this experiment this was not possible. Cementing the annulus with low impedance cement should yield a lot higher flexural wave attenuation, and would confirm the results in this thesis. Make sure to fill the annulus with water after cementing.

Creating a good model in COMSOL Multiphysics would greatly aid the future work. Predicting arrival times and wave paths from the physical experiments becomes a lot easier with the addition of simulation results. What Lamb-modes are excited in the steel plate is almost impossible to tell from the experiment measurements and require numerical simulation. Using a frequency transducer of around 250kHz is recommended to future work because it would excite less higher-order modes and create a stronger flexural wave.

A | Abbreviations

P&A	Plug and abandonment
CET	Cement Evaluation Tool
PET	Pulse Echo Tool
USI	Ultrasonic Imager
CAST-V	Circumferential Acoustic Scanning Tool-Visualization
IMS	Inspection and Measuring Systems
NDT	Non-Destructive Testing
DPO	Digital Phosphor Oscilloscope
MUSA	Matlab Ultrasonic Analyser
BeCaLoS	Behind Casing Logging Set-up
TIE	Third Interface Echo
P-E	Pulse-Echo
P-C	Pitch-Catch

Bibliography

[1] Allouche, M., Guillot, D., Hayman, A. J., Butsch, R. J., and Morris, C. W. (2005a). *Well Cementing*, chapter 15, Cement Evaluation. Schlumberger.

[2] Allouche, M., Guillot, D., Hayman, A. J., Butsch, R. J., and Morris, C. W. (2005b). *Well Cementing*, chapter 5. Schlumberger.

[3] Calvert, D. (2005). *Well Cementing*, chapter Preface. Schlumberger.

[4] Froelich, B. and Zeroug, S. (2003). Ultrasonic leaky-lamb wave imaging through a highly contrasting layer. In *IEEE Ultrasonic Symposium*.

[5] Hayden, R., Russel, C., Vereide, A., Babasick, P., Shaposhnikov, P., and May, D. (2011). Case studies in evaluation of cement with wireline logs in a deep water environment. In *SPWLA 52nd Annual Logging Symposium*. Schlumberger, SPWLA.

[6] Hayman, A. J., Hutin, R., and Wright, P. V. (1991). High-resolution cementation and corrotion imaging by ultrasound. In *SPWLA 32nd Annual Logging Symposium*. Society of Petrophysicists and Well-Log Analysts.

[7] Holt, R. M., Larsen, I., and Li, L. (2004). Estimation of intergranular bond strengths by core scratching: A comparison between a laboratory experiment and a numerical discrete particle simulation. *North American Rock Mechanics Symposium*.

[8] Hovem, J. M. (2012). *Marine Acoustics: The Physics of Sound in Underwater Environments*. Peninsula Publishing.

[9] Kuttruff, H. (1991). *Ultrasonics: Fundementals and applications*. Elsevier.

[10] Løvstad, A. (2012). *Detection of localised corrosion in pipes using guided waves*. PhD thesis, NTNU.

[11] Mindlin, R. D. (1951). Influence of rotatory inertia and shear on flexural motions of isotropic, elastic plates. *ASME Journal of Applied Mechanics*, 18:31–38.

[12] Morris, C., Vaeth, J., van Kuijk, R., and Froelich, B. (2007). Application of enhanced ultrasonic measurements for cement and casing evaluation. In *SPE/IADC Drilling Conference*. Society of Petroleum Engineers.

[13] NDT-Education (2001). Introduction to ultrasonic testing. http://www.ndt-ed.org/EducationResources/CommunityCollege/Ultrasonics/cc_ut_index.htm.

[14] Olympus-IMS. Immersion flaw detectors. www.olympus-ims.com/en/ultrasonic-transducers/immersion/?search#cmsContent4163.

[15] Reissner, E. (1945). The effect of transverse shear deformation on the bending of elastic plates. *ASME Journal of Applied Mechanics*, 12:A68–77.

[16] Schlumberger (2011). Isolation scanner - advanced evaluation of wellbore integrity product brochure.

[17] van Kuijk, R., Zeroug, S., Froelich, B., Allouche, M., Bose, S., Miller, D., le Calvez, J.-L., Schoepf, V., and Pagnin, A. (2005). A novel ultrasonic cased-hole imager for enhanced cement evaluation. Number IPTC 10546. Schlumberger, IPTC.

[18] Vigran, T. E. (2002). *Bygningsakustikk – et grunnlag*, chapter 3, pages 79–82. Tapir Akademisk Forlag.

[19] Wikipedia (2014). Lamb waves. http://en.wikipedia.org/w/index.php?title=Lamb_waves&oldid=578626979.